Study of Numerical Stochastic Perturbation Theory toward the high-order perturbation of matrix models

(行列模型の高次摂動計算のための数値確率過程摂動理論の研究)

Hiroshima University,
Graduate School of Advanced Science and Engineering,
Physics Program(Doctoral Course)

Yingbo Ji

A thesis for the degree of Doctor of Philosophy

February 2024

Abstract

In this thesis, I study the high-order perturbative behavior of a QCD-like matrix model called the twisted reduced principal chiral model using numerical stochastic perturbation theory (NSPT). Recently, resurgence theory in mathematics has provided a way to extract non-perturbative information, such as instantons and renormalons, from perturbation theory by recognizing the divergent perturbative series that carries non-perturbative effects in its asymptotic behavior in some quantum mechanics and quantum field theories. Consequently, we could extract the non-perturbative component, provided we possess sufficiently high-order perturbative coefficients. This task proves challenging using conventional methods such as Feynman diagrams, as the number of diagrams exhibits factorial divergence with a given perturbative order. One way to alleviate this is called NSPT. Even though NSPT reduces the computational cost from $\mathcal{O}(N_{PT}!)$ to $\mathcal{O}(N_{PT}^2)$, where N_{PT} represents the maximum truncated order in perturbation calculation, it still requires considerable computational time to achieve it. In this thesis, I developed a new algorithm called the Paterson-Stockmeyer (P-S) method to accelerate the bottleneck of the NSPT simulation. Moreover, using the newly developed method combined with large N factorization, I have investigated the high-order perturbative behavior of TRPCM and observed a signal indicating the existence of renormalons in the numerical results. In conclusion, I extracted non-perturbative information using high-order calculations of perturbative coefficients for this specific model. The same workflow can be applied to other complicated theories, such as full QCD, which is our target, yielding similar results.

Contents

1 Introduction

Quantum Chromodynamics (QCD) [1] is a gauge theory based on the $SU(3)$ group and is an asymptotically free theory, which means that the interactions between quarks become weak at small distances. Due to asymptotic freedom, it is possible to carry out perturbative calculations in the weak coupling regime. However, until 1974, most studies of QCD were limited to perturbation theory.

In 1974, a breakthrough occurred with two famous papers that aimed to unravel the mysteries of QCD, particularly quark confinement. One was by 't Hooft, considering the large N (number of colors) limit of QCD. The other was by Wilson, who discretized the continuum theory, establishing the lattice method to enable non-perturbative studies of QCD.

The first paper, titled "A planar diagram theory for strong interactions" [2] was written by Gerard 't Hooft. In this work, 't Hooft considered a pure Yang-Mills model with the number of colors, denoted as N, set to infinity, while keeping the coupling constant g equal to zero. Instead, he held the newly defined 't Hooft coupling, Ng^2, as a constant. Using this approach, Feynman diagrams could be organized in terms of a so-called $1/N$ expansion. In the large N limit, only the leading term, which is independent of N, remains. This mathematical simplification motivated many researchers in the field. Eguchi and Kawai investigated the large N limit of the $SU(N)$ Yang-Mills theory defined on the lattice. They pointed out that the elimination of space-time dependence occurs, leading to matrix models referred to as the Eguchi-Kawai model or reduction [3]. Not only is it mathematically elegant, but ignoring the space-time dependency in our numerical simulations means that we can save a lot of computational resources in terms of memory and CPU time. However, it didn't last long. Okawa showed that the Z_N symmetry is simultaneously breaking in the weak coupling region numerically using Monte Carlo method [4]. Okawa and González-Arroyo subsequently replaced the periodic boundary conditions (PBCs) with twisted boundary conditions (TBCs), and the newly developed reduced model, named the twisted Eguchi-Kawai (TEK) model, could reproduce all results in both the weak and strong coupling regions [5, 6].

In the second paper, titled "Confinement of quarks" [7], Kenneth Wilson introduced a lattice

regularization for QCD. This approach involved discretizing the continuum theory on a lattice and provided a way to prove the confinement of quarks in the strong coupling limit. These studies soon evolved and gave rise to what is now known as lattice field theory, leading to a significant expansion of research into the properties of QCD in the strong interaction regime. Prior to these developments, most research in this field relied on analytic methods. While elegant in terms of mathematics, these methods had their limitations.

The use of numerical techniques, such as Markov Chain Monte Carlo (MCMC), for studying statistical systems was already in existence. Kenneth Wilson and others adapted these techniques to study lattice gauge theories in a non-perturbative manner. One pioneering work was done by Michael Creutz [8], who used the Monte Carlo method to study $U(1)$ [9] and $SU(2)$ [10] pure gauge theories, numerically demonstrating confinement of quarks in $SU(3)$ pure gauge theoires [11]. Subsequently, numerous numerical algorithms were developed and successfully applied to lattice QCD [12]. These algorithms include the Langevin algorithm [13], the Molecular Dynamics method [14], and the Hybrid Monte Carlo method [15], whose origin is from the Langevin algorithm. With the combined use of these algorithms and the increasing computational resources available, studies in lattice QCD transformed into their present form, which involves a combination of analytic calculations and increasingly large-scale numerical simulations. As these techniques have advanced, lattice methods have become a highly accurate and essential source for calculations within the standard model and for investigations beyond the standard model in the field of particle physics [16, 17].

Using numerical methods in a non-perturbative manner has been instrumental in extracting crucial information from QCD. However, perturbative information is still important, particularly when studying high-order perturbation behavior [18, 19]. The traditional Feynman diagram-based method can be a good choice for lower-order calculations, such as those involving one-loop or two-loop diagrams.

However, when it comes to high-order calculations, the diagram-based approach becomes computationally expensive. To calculate the perturbative coefficients at the n-th order, the number of diagrams that need to be considered grows factorially, making it impractical for very high or-

ders. This computational explosion makes it difficult to analytically verify results obtained through physical intuition or heuristic arguments, especially when dealing with high-order behavior. As a result, researchers often rely on numerical simulations and advanced computational techniques to explore and understand the behavior of QCD, while seeking to find efficient methods for handling high-order perturbative calculations.

Fortunately, an alternative approach to tackle this problem exists, known as Stochastic Quantization and Numerical Stochastic Perturbation Theory [20, 21, 22]. In 1981, Parisi and Wu introduced a novel method to formulate perturbative expansions for quantum field theory. They achieved this by extending a d-dimensional field theory to a $d+1$-dimensional one, introducing an extra dimension denoted as t, and starting from the Langevin equation. As this extra dimension t tends towards infinity, the non-equilibrium distribution converges to the equilibrium distribution, ultimately reproducing the results of quantum field theory.

The perturbative version of this approach, known as stochastic perturbation theory, involves expanding all variables in terms of the coupling constant and rearranging the Langevin equation order by order. In 1993, Renzo and his collaborators further advanced stochastic perturbation theory to the numerical stochastic perturbation theory (NSPT), applied to the lattice field theory, by discretizing the additional dimension and implementing the Langevin equation on a computer [23]. This computational approach enabled the exploration of perturbative behavior in quantum field theory. The significant advantage of NSPT over the diagram method is that the computational complexity of computing an expansion up to order n is proportional to n^2 and not to $n!$, which allows for perturbation calculations to be performed to much higher orders.

The 4-dimensional QCD and its corresponding TEK model provide an excellent starting point for studying various interesting features of physics in the real world. However, these models are highly complex, and directly studying them in both numerical and analytical aspects poses significant challenges. Fortunately, a simpler model known as the two-dimensional Principal Chiral Model (PCM) is often considered a toy model for four-dimensional pure gauge theory because it shares many interesting properties with it [24, 25, 26, 27, 28, 29, 30, 31, 32, 33]. These properties include generating a mass gap [34] and asymptotic freedom.

To study these properties, various perturbative and non-perturbative methods have been applied [33, 35]. One such method is the large N expansion in terms of 't Hooft coupling, which can be applied to both the PCM and gauge theories. It involves reorganizing the standard weak-coupling expansion to obtain better behavior and simplify Feynman diagrams to explain the perturbative properties of the theories. The lattice method has also been applied to these models to study non-perturbative properties. Combining the lattice method with the large N expansion is a natural approach to understand the origin of these properties.

Exploring the lattice PCM at large N is an important step toward understanding four-dimensional lattice gauge theories. Similar to four-dimensional lattice gauge theories, the two-dimensional PCM has a reduced version called TRPCM short for twisted reduced principal chiral model [36, 37]. One advantage of TRPCM is that there's no need to consider the model in several different volumes and then perform the model in infinite volume using that data, once taking the large N limit.

Studying the high-order perturbative behavior of TRPCM at the large N limit is an important pursuit, as it is known that perturbation expansions are asymptotic in most quantum field theories and quantum mechanics [38]. The large order behavior of these series could potentially shed light on the non-perturbative effects of the corresponding theory. Renormalons [39, 40] and their applications provide examples of how the asymptotic series are connected to non-perturbative contributions, and these have been extensively studied in QCD and QCD-like theories.

Recent developments in resurgence theory [41, 42] have further connected asymptotic behavior to non-perturbative objects, such as the complex saddle points of the action in certain models, for example the two-dimensional 2D CP^N sigma model [43, 44] and three-dimensional Chern-Simons theory [45]. This has opened up new avenues for understanding the relationship between perturbative and non-perturbative aspects of quantum field theories.

Investigating the high-order behavior of TRPCM in the large-N limit indeed holds the promise of simplifying the perturbation series and revealing its connection to non-perturbative phenomena. To extract non-perturbative effects from the perturbation series, understanding the behavior of coefficients as a function of the expansion order in terms of the coupling constant g at relatively

high orders is of utmost importance. The specific order at which the perturbative series exhibits divergent behavior depends on the observable being studied and the renormalization scheme of the coupling. This complexity makes the task challenging, especially for models that are not analytically solvable, and highlights the necessity of employing numerical methods to make progress.

To achieve the goal of extracting non-perturbative information from the perturbative series, we have implemented the NSPT method for TRPCM to study interesting properties, such as the large N factorization and $1/N$ correction. This endeavor aims to provide valuable insights into whether renormalons exist in the large N limit and how to extract non-perturbative information from the perturbative series. Once successful, this workflow can be extended to apply to the TEK model, potentially yielding valuable information that reflects real-world phenomena.

Meanwhile, certain studies aim to establish the presence of non-perturbative effects using perturbation theory. A notable achievement, closely connected to our recent work, is credited to Bruckmann and Puhr [46]. They conducted their investigation on the lattice for the PCM, specifically focusing on this model with a restricted number of colors (ranging from 3 to 6) and employing high-order calculations. Through the analysis of high-order perturbative coefficients, they indirectly revealed signal of renormalons by monitoring the ratio of adjacent coefficients. In contrast to their methodology, our emphasis lies in the examination of both the large N and high-order behavior of the TRPCM, which is essentially equivalent to the $SU(N = \infty)$ PCM in the continuum limit. As mentioned earlier, the advantage of considering the large N limit extends beyond its simplification in mathematical formulations; it also encompasses unique properties such as large N factorization in numerical simulations. This approach enables us to investigate whether the renormalons exist in the large N limit.

The contents of the thesis are organized as follows: In Section 2, we review the basic ideas and important properties of the PCM and TRPCM. In Section 3, we provide an overview of Parisi-Wu stochastic quantization applied to numerical calculations in lattice field theory, along with its numerical application, NSPT. We also present some details about a new method we recently developed, called the P-S method, which accelerates NSPT simulations. Section 4 is dedicated to presenting numerical results from NSPT simulations of TRPCM and a benchmark of the P-S

method. Finally, in Section 5, we offer a brief summary of the thesis and discuss potential future research directions.

2 Twisted Reduced Principal Chiral model

In this section, we will commence by reviewing some aspects of PCM in both continuum and lattice formulations, as well as the physical observable of our interest. Due to the perturbation series' inherently asymptotic nature, we will also delve into examining the asymptotic behavior, commonly referred to as renormalons, [40, 46, 47] within the PCM framework. In the final subsection, we will explore fundamental concepts in TRPCM.

2.1 Principal chiral model and lattice version

The $SU(N)$ PCM is a quantum field theory with a Lagrangian density defined as follows

$$L = \frac{1}{g^2} \operatorname{Tr} \left(\partial_\mu U(x) \partial_\mu U^\dagger(x) \right), \tag{1}$$

where the field variable $U(x)$ belongs to the fundamental representation of the $SU(N)$ group. In a two-dimensional case, the theory exhibits asymptotic freedom and generates a mass gap, which is similar to the 4-dimensional Yang-Mills theory. The theory maintains invariance under the following transformation:

$$U(x) \longrightarrow \Omega' U(x) \Omega^\dagger, \tag{2}$$

where Ω and Ω' are $SU(N)$ group matrices.

Since formulating the model on the lattice opens the door to a non-perturbative exploration of its properties and other phenomena, in this context, the partition function is expressed as follows:

$$Z = \int \prod_n dU(n) \exp\{-bN \sum_n \sum_\mu \operatorname{Tr}(\delta_\mu U(n) \delta_\mu U^\dagger(n))\}, \tag{3}$$

where $\delta_\mu U(n) = U(n + \hat{\mu}) - U(n)$ represents the discretized derivative, n is the two dimensional site index and $\hat{\mu}$ shows an unit vector in the μ direction. The parameter $b = 1/(g^2 N)$ serves as the inverse of the lattice 't Hooft coupling.

The main observable in the lattice model is the internal energy (E) which can be expressed as

follows

$$a^2 E = \frac{1}{2N}\langle \sum_{\mu,n} \mathrm{ReTr}\left[\delta_\mu U(n)\delta_\mu U^\dagger(n))\right]\rangle, \tag{4}$$

where a is the lattice spacing and the expectation value, denoted as $\langle \cdots \rangle$, is defined by considering this path integral measure for an observable $\mathcal{O}[U]$ as:

$$\langle \mathcal{O} \rangle = \frac{1}{Z}\int_n dU(n)\mathcal{O}[U]e^{-S[U]}. \tag{5}$$

2.2 Renormalons in PCM

The internal energy defined in Eq. (4) can be represented in the following derivation form

$$a^2 E = 1 - \frac{1}{4N^2 V}\frac{\partial \log Z}{\partial b}, \tag{6}$$

where V represents lattice volume. In order to establish a basis for understanding the renormalon behavior in the internal energy, we can draw upon the large N expansion framework to show the relation between the a, the resulting intrinsic scale Λ_L, which has strong relation with the mass gap and the coupling constant b through a two-loop renormalzation group relation

$$\begin{aligned} a\Lambda_L =& \sqrt{8\pi b}\exp(-8\pi b) \quad (b \to \infty) \\ =& (b/\beta_0)^{\beta_1/\beta_0^2}\exp\left(-b/\beta_0\right), \\ \beta_0 =& \frac{1}{8\pi}, \quad \beta_1 = \frac{1}{128\pi^2}, \end{aligned} \tag{7}$$

where β_0 and β_1 are the first and second expansion coefficients of beta-function. On the other hand, combining operator product expansion (OPE) and Eq. (7) indicates the existence of exponentially small non-perturbative term in the weak coupling expansion and then can lead to the high-order

perturbative behavior of the internal energy as

$$a^2 E = \sum_{n=0}^{\infty} E^{(n)} b^{-n} + c e^{-2b/\beta_0}. \tag{8}$$

The second term comes from the renormalization group behavior of a^2 factor. From a non-perturbative aspect, $a^2 E$ is defined for $1/b$, but the first term in the perturbation series is not convergent series but a asymptotic series. To avoid the inconsistency between the non-perturbative form and the perturbaitve one, the asymptotic series should behave as

$$E^{(n)} \overset{n\to\infty}{\sim} \left(\frac{\beta_0}{2}\right)^n n!, \quad \frac{\beta_0}{2} = \frac{1}{16\pi}, \tag{9}$$

which means that the perturbative coefficients become factorially divergent in the higher order case which is about 50 order in the 't Hooft coupling expansion and before that the coefficients will decrease gradually. In addition, since there is no alternative sign in Eq. (9), the Borel transformation of the series will led a pole (singularity), named renormalons as it emerges from the renormalization process, located on the real positive axis in the Borel plane, which gives a non-perturbative ambiguity, indicating the existence of the second term. The definition of $a^2 E$ should be unambiguous, ensuring that any ambiguity arising from the perturbative series is eliminated by incorporating the non-perturbative effects as anticipated by the renormalons arguments.

Even the typical expression of the internal energy has not been proven in TRPCM, but in some quantum mechanical models or other simpler quantum field theory models the existence of typical trans-series expansion of the main observable $\mathcal{O}$ has been proven using the resurgence theory as

$$\mathcal{O}(b) \sim \sum_{k=0}^{\infty} c_{(0,k)} (b)^{-k} + \sum_{n=1}^{\infty} (b)^{\beta_n} e^{-nAb} \sum_{k=0}^{\infty} c_{(n,k)} (b)^{-k}, \tag{10}$$

where the first sum is the asymptotic series and the second term shows non-perturbative contributions from the n-instantons or complex saddle points [42]. We hope the same thing happens in PCM and TRPCM. In order to do that, one need to calculate the perturbative coefficients and

re-sum the series using special method like Borel re-summation [48].

2.3 Twisted reduced principal chiral model

The twisted reduced principal chiral model is a single matrix model. In its large N limit, it is suggested to be equivalent to the standard lattice version of the lattice PCM at infinite volume or the PCM in continuum theory. This equivalence is realized by absorbing space-time dependency into specific $SU(N)$ matrices Γ_μ called twist matrix. The partition function therefore becomes

$$Z = \int dU \ \exp\{-bN \sum_\mu \mathrm{Tr}(\Delta_\mu U \Delta_\mu U^\dagger)\}, \tag{11}$$
$$\delta_\mu U \rightarrow \Delta_\mu U \equiv \Gamma_\mu U \Gamma_\mu^\dagger - U.$$

In 2-dimensional case, the choice of Γ_μ is based on the 't Hooft algebra and abides by the following relation

$$\Gamma_1 \Gamma_2 = \exp\{\frac{2\pi i K}{N}\} \Gamma_2 \Gamma_1, \tag{12}$$

where a hyperparameter K, called flux parameter, was introduced. K plays an important role in realized with the equivalences between the reduced model and PCM at continuum limit. The dependency of K flux parameter has been investigated in several works [37, 49, 50]. A minimal choice, which means that holding $K = 1$ fixed as N becomes large, often leads to the breaking of central symmetry in weak coupling region and spoils the equivalence of the large N limits of the lattice chiral model and the corresponding TEK reduction [51]. To keep the equivalence, K should be changed according to the following conditions given in [37] as

$$\frac{K}{N} > \Lambda,$$
$$Mod(K\bar{K}, N) = 1, \tag{13}$$
$$\frac{\bar{K}}{N} \quad \text{holds almost same for different } N.$$

One typical choice of (N, K) pair can be determined from the Fibonacci series with

$$K = F_{n-2} = \bar{K}, \tag{14}$$

$$N = F_n, \tag{15}$$

where n represents the n-th number in the Fibonacci series. This choice has been shown to be reasonable in other models, and thus we follow this choice with $(N, K) = (55, 21), (89, 34), (144, 55)$ and $(233, 89)$.

The internal energy in the reduced model can be modified using the Γ_μ as

$$E = \frac{1}{2N} \sum_{\mu} \mathrm{Re}\,\mathrm{Tr}\left[U\Gamma_\mu U^\dagger \Gamma_\mu^\dagger\right]. \tag{16}$$

We have introduced the PCM and TRPCM along with some interesting properties of these models. In the following sections, we will study both the large N and perturbative behavior of the TRPCM using a numerical approach. Our primary goal is to explore the large N limit and the high-order behavior to investigate the existence of renormalons. The renormalon behavior of PCM has been demonstrated in Section 2.2, and TRPCM exhibits the same property in the large N limit.

One significant advantage of TRPCM over PCM is that, unlike PCM, there is no need to consider double limits—the large N limit and the infinite volume limit. In TRPCM, when taking the large N limit as $N \to \infty$, the effective volume, which functionally depends on N (usually $N^2 = L^2 = V$), automatically becomes infinite. In contrast, in the lattice PCM case, to achieve the infinite volume limit, one must simulate the model in a finite lattice volume and then extrapolate to the infinite volume with the help of the renormalization group equations—a process that can be quite complicated.

This simplification is not only appreciated in theoretical terms but also serves as a practical alternative in numerical simulations, as it reduces memory usage and speeds up computations. To illustrate, consider an example of a $SU(233)$ TRPCM and the corresponding $SU(233)$ PCM defined on a 233×233 square lattice. The memory usage of PCM is approximately 10^5 times larger than that of TRPCM. As we consider larger values of N, the difference becomes even more

remarkable.

For these reasons, in the next section, we will introduce the numerical method we will use to study TRPCM and explain how to adapt the numerical method to be compatible with TRPCM.

3 Stochastic quantization and Numerical Stochastic Perturbation Theory

In the realm of theoretical physics, quantization serves as the pivotal bridge connecting classical physics with the enigmatic world of quantum physics. This process is often achieved through various methodologies, with Canonical quantization and the path integral, introduced by the illustrious R. Feynman. However, in 1981, G. Parisi and Y.-S. Wu introduced an alternative method [20], called Stochastic Quantization, for tackling this profound challenge. Their method set its foundation on the Langevin equation describing the approach to equilibrium. What makes this approach truly remarkable is its versatility, as it can be readily applied to a wide range of problems, spanning from quantum mechanics to quantum field theories.

Moreover, when we introduce a perturbative expansion for field variables within this framework, we obtain Stochastic Perturbation Theory (SPT). The solubility of the Langevin equation on a computer and the remarkable advancements in computational capacity have allowed F. Renzo and his collaborators to push the study further. They have developed the NSPT [52], a numerical approach built on the top of SPT. This numerical adaptation empowers us to evaluate complex perturbative calculations of various physical variables in a semi-automated fashion, leveraging the computational power of modern technology.

Subsequent to these developments, a flurry of research has emerged, with a focus on utilizing NSPT to explore models that were previously uncharted territory where traditional Feynman diagram-based methods can not achieve [46, 47, 52, 53, 54, 55, 56, 57, 58, 59]. Additionally, other researchers have embarked on the mission of refining and extending algorithms to enhance the efficiency and capabilities of this powerful approach [60, 61].

In this chapter, our thesis begins with an introduction to stochastic quantization and SPT. As the NSPT is built on the top of stochastic quantization, we delve into the fundamental concepts underpinning the NSPT algorithm. We will pay special attention to the molecular dynamics-based NSPT and explore the intricacies of applying NSPT to the TRPCM, a model of particular our interest. Lastly, we will show the latest algorithms we have developed to accelerate the NSPT

simulations to improve efficiency and effectiveness.

3.1 Stochastic quantization and numerical stochastic perturbation theory

We consider a quantum field theory defined in Euclidean space. The partition function and the expectation value of a physical observable, denoted as $\mathcal{O}(\varphi)$, can be expressed in the form of a path integral as follows:

$$Z = \int d\varphi(x) e^{-S(\varphi,g)}, \tag{17}$$

$$\langle \mathcal{O}(\varphi) \rangle = \frac{1}{Z} \int d\varphi(x) \mathcal{O}(\varphi) e^{-S(\varphi,g)}, \tag{18}$$

where $\int d\varphi(x)$ represents the path integral measure, and $S(\varphi, g)$ encompasses the field φ and the coupling constant g, which signifies the system's interaction.

We start with the Langevin equation to evaluate the evolution of the field non-perturbatively:

$$\frac{\partial \varphi(x,t)}{\partial t} = -\frac{\partial S(\varphi, g)}{\partial \varphi(x)}\bigg|_{\varphi(x)=\varphi(x,t)} + \eta(x,t), \tag{19}$$

where the η is a set of independent Gaussian distributed noise for each lattice site x and Langevin time t which satisfies

$$\begin{aligned} \langle \eta(x,t) \rangle &= 0, \\ \langle \eta(x,t)\, \eta(x',t') \rangle &= 2\delta(x-x')\delta(t-t'). \end{aligned} \tag{20}$$

The introduction of $\eta(x,t)$ to the system imparts a stochastic nature to the process, rendering the time-dependent variable $\varphi(x,t)$ stochastic. This stochastic nature is implicit and is contingent upon $\eta(x,t)$. The estimation of the expectation value, as expressed in Eq. (18), proceeds as follows

$$\lim_{t\to\infty} \langle \mathcal{O}(\varphi(x,t)) \rangle_\eta = \langle \mathcal{O}(\varphi(x)) \rangle, \tag{21}$$

where $\langle \cdots \rangle_\eta$ represents the statistical ensemble average concerning the stochastic variable $\varphi(x,t)$ generated through the solution of Equation (19). The non-perturbative expectation value is achieved in the limit of infinite Langevin time.

In this thesis, our objective is to perturbatively evaluate Eq (18) by expanding it in terms of the coupling constant g. The traditional expansion of the coupling constant within the path integral formulation introduces the well-known Feynman diagram method. However, as we move to high-order expansions, the evaluation, both diagrammatically and algebraically, becomes increasingly challenging.

To address this, we employ the NSPT method, which is formulated on top of the Langevin equation (19) by expanding it with respect to g. Consequently, we will derive the perturbative version of the Langevin equation.

As a prerequisite, we assume that the total action can be decomposed into two components: a free action part, denoted as $S_0(\varphi)$, which is usually assumed to be a quadratic function of ϕ, and an interaction action part, $S_{int}(\varphi, g)$, which contains a polynomial of ϕ in terms of g. Additionally, we expand the field variable $\varphi(x,t)$ as a function of g, recognizing that its implicit dependence on g stems from the solution of Eq. (19);

$$S\left(\varphi, g\right) = S_0 + S_{int}, \tag{22}$$

$$S_0 = \int dx \varphi(x) \Delta(x,y) \varphi(y), \tag{23}$$

$$\varphi\left(x,t\right) = \sum_{n=0}^{\infty} g^n \varphi_n(x,t). \tag{24}$$

where $\Delta(x,y)$ shows the free part of the action and usually contains the kinetic and mass term. By substituting Eq. (22) and Eq. (24) into Eq. (19) and organizing the terms according to their respective orders of g^n in Eq. (19), we derive the following set of differential equations;

$$\frac{\partial \varphi_0(x,t)}{\partial t} = - \left. \frac{\partial S_0}{\partial \varphi(x)} \right|_{\varphi(x)=\varphi_0(x,t)} + \eta(x,t) \tag{25}$$

$$\frac{\partial \varphi_n(x,t)}{\partial t} = - \left. \frac{\partial S_0}{\partial \varphi(x)} \right|_{\varphi(x)=\varphi_n(x,t)} + I_n\left(\varphi_0, \ldots, \varphi_{n-1}\right) \text{ for } n \geq 1, \tag{26}$$

where we have two types of differential equations. The first equation, denoted as Eq. (25), incorporates the Gaussian noise $\eta(x,t)$, which is accountable for quantum fluctuations. The solution for

this equation can be expressed as:

$$\varphi_0\left(x,t\right)=\int_0^t d\tau\int dyG\left(x-y,t-\tau\right)\eta\left(y,\tau\right), \tag{27}$$

whihc implies that the solution $\varphi_0(x,t)$ also becomes a stochastic variable. In the second equation, represented as Eq. (26), $I_n(\varphi_0,\ldots,\varphi_{n-1})$ can be derived by expanding the interaction action S_{int} according to the expansion rule provided in Eq. (24). The term $G(x-y,t-\tau)$ corresponds to Green's function, which can be obtained from Eq. (25) by substituting φ with $G(x-y,t-\tau)$, as follows:

$$\frac{\partial G\left(x-y,t-\tau\right)}{\partial t}+\left.\frac{\partial S_0}{\partial\varphi(x)}\right|_{\varphi(x,t)\to G(x-y,t-\tau)}=\delta(x-y)\delta(t-\tau). \tag{28}$$

It is important to note that $I_n(\varphi_0,\ldots,\varphi_{n-1})$ depends only on those fields for which the order is less than n, which means that the simulation process can be truncated at any order we choose.

By numerically solving these hierarchical equations, specifically the hierarchical differential equations (25) and (26), we can generate the statistical ensemble for $(\varphi_0(x,t),\varphi_1(x,t),\ldots,\varphi_n(x,t))$. These stochastic variables are then employed for evaluating observable.

The expectation value of any physical observable ($\mathcal{O}(\phi(x,t))$) associated with the variable $\varphi(x,t)$ can be expanded in a manner analogous to what we have employed for the variable φ;

$$\langle\mathcal{O}\rangle=\left\langle\sum_{n=0}g^n\mathcal{O}_n\right\rangle=\sum_{n=0}c_n(\mathcal{O})g^n. \tag{29}$$

$\mathcal{O}_n$ becomes a function of the stochastic variables $(\varphi_0(x,t),\varphi_1(x,t),\ldots,\varphi_n(x,t))$, and $c_n(\mathcal{O})$ is determined as follows:

$$c_n(\mathcal{O})=\lim_{t\to\infty}\langle\mathcal{O}_n(\varphi_0(x,t),\varphi_1(x,t),\ldots,\varphi_n(x,t))\rangle_\eta. \tag{30}$$

3.2 Simulation methods and its application to TRPCM

In this thesis, we employ a Hybrid Molecular Dynamics (HMD) approach within NSPT. The HMD method has been employed to investigate a wide range of complicated and non-local systems

in non-perturbative fashion. Significantly, its extension, the Hybrid Monte Carlo (HMC) method, has garnered substantial significance due to its computational efficiency and enhanced ergodicity.

Applying HMD to NSPT is a natural means of enhancing the efficiency of NSPT. Further advancements in NSPT beyond HMD have been explored in Ref. [61].

To naturally advance the development of HMD-based NSPT, we initiate with a non-perturbative simulation of TRPCM. Beginning with the HMD simulation for TRPCM, the partition function for the HMD-based Monte Carlo algorithm is derived from Eq. (11) by introducing a $N \times N$ traceless Hermitian matrix P conjugated to U as

$$Z = \int \mathrm{d}U \, \mathrm{d}P \, e^{-H[P,U]}, \tag{31}$$

$$H[P,U] = \frac{1}{2}\mathrm{Tr}\left[P^2\right] + S[U], \tag{32}$$

where the variables P and U are stochastically generated to conform to the probability density $\mathrm{d}U \, \mathrm{d}P \, e^{-H[P,U]}/Z$ in the HMD algorithm. The Markov chain for the density is established by treating $H[P,U]$ as a Hamiltonian and introducing a fictitious time t for the dynamic variables P, U. The classical Hamiltonian equations for TRPCM are derived as

$$\frac{\mathrm{d}U}{\mathrm{d}t} = iPU, \quad \frac{\mathrm{d}P}{\mathrm{d}t} = F, \tag{33}$$

$$F = ibN\left(V - \frac{1}{N}\,\mathrm{Tr}\,[V]\right), \quad V = UX - (UX)^\dagger, \tag{34}$$

$$X = \sum_\mu \left[\Gamma_\mu^\dagger U^\dagger \Gamma_\mu + \Gamma_\mu U^\dagger \Gamma_\mu^\dagger\right]. \tag{35}$$

The HMD algorithm employs a symplectic integration scheme to approximate the time evolution of the equation of motion (33). The variable P is periodically refreshed as a stochastic variable from a Gaussian distribution $\exp[-\,\mathrm{Tr}\,[P^2]/2]$ at each beginning of the trajectory that is defined by a fixed time length period. The Markov Chain Monte Carlo sampling in the HMD algorithm involves periodic sampling from the trajectory of P, U as a function of time t.

The HMD-based NSPT is derived by substituting the variables P, U into Eq. (33), incorpo-

rating their perturbative expansion in terms of the coupling constant. For the ease of handling the large N limit of the TRPCM, the 't Hooft coupling, represented as $\lambda \equiv b^{-1}$, functions as a natural expansion parameter. We show the perturbative expansion for U and P which is delineated as follows:

$$U = \sum_{k=0}^{\infty} \lambda^{k/2} U^{(k)}, \quad P = \lambda^{-1/2} \sum_{k=1}^{\infty} \lambda^{k/2} P^{(k)}, \tag{36}$$

where $U^{(0)} = I$ and $P^{(0)} = 0$ are initial conditions and imposed as the perturbative vacuum and non-dynamical variable. The initial coefficient of P, denoted as $P^{(1)}$, acts as the source of the stochastic process and is generated from a Gaussian distribution $\exp\left[-\operatorname{Tr}\left[\left(P^{(1)}\right)^2\right]/2\right]$. In contrast, the higher-order coefficients, $P^{(k)}$ for $k > 1$, are reset to zero at the beginning of each trajectory.

Since the force F initiates at $\mathcal{O}(\lambda^{-1})$, we shift the expansion of P by $\lambda^{-1/2}$ and adjust the unit of the fictitious time as

$$t = \lambda^{1/2} t'. \tag{37}$$

For the sake of simplicity, we will omit the prime symbol for the rescaled time unit hereafter. The fundamental components of the symplectic time integration scheme are:

$$U^{(k)}(t + \delta t) = \left[e^{iP\delta t} \circledast U(t)\right]^{(k)}, \tag{38}$$

$$P^{(k)}(t + \delta t) = P^{(k)}(t) + F^{(k)} \delta t, \tag{39}$$

where δt represents the discretized time step. In Eqs. (38) and (39) , the integration time step of δt can be chosen arbitrary, depending on the integration scheme being used. The symbol $\circledast$ indicates

the polynomial convolution product for two matrix polynomials as

$$A = \sum_{i=0}^{\infty} g^i A^{(i)}, B = \sum_{i=0}^{\infty} g^i B^{(i)}, C = \sum_{i=0}^{\infty} g^i C^{(i)}, \tag{40}$$

$$C = AB \to C^{(k)} = (A \circledast B)^{(k)} = \sum_{l=0}^{k} A^{(l)} B^{(k-l)}, \tag{41}$$

where $A^{(i)}, B^{(i)}, C^{(i)}$ are matrix-valued coefficients of matrices A, B, C. Calculating the perturbative expansion for the matrix exponential $e^{iP\delta t}$ in Eq.(38) is a crucial aspect of NSPT simulation. This significance arises not only due to its intricate definition but also because, in our simulations, we observe that nearly half of the computational time is dedicated to this calculation. Recognizing this, we have devised a rapid algorithm for its computation[62] and provided a more detailed explanation of the definition of $e^{iP\delta t}$ and the expedited computation of $e^{iP\delta t}$in the subsequent subsection. The perturbative expansion of the force F is obtained as follows:

$$F^{(k)} = iN \left(V^{(k)} - \frac{1}{N} \mathrm{Tr} \left[V^{(k)} \right] \right), \quad V^{(k)} = S^{(k)} - S^{(k)^\dagger}, \tag{42}$$

$$S^{(k)} = (U \circledast X)^{(k)}, \quad X^{(k)} = \sum_{\mu} \left[\Gamma_\mu^\dagger U^{(k)\dagger} \Gamma_\mu + \Gamma_\mu U^{(k)\dagger} \Gamma_\mu^\dagger \right]. \tag{43}$$

It is worth noting that the HMD algorithm for NSPT has been observed to exhibit non-ergodic behavior, as discussed in references such as Refs. [63, 64, 61, 65]. To address this non-ergodicity, two remedies have been established. One approach involves systematically sampling all Fourier modes of field variables by introducing random variations in the trajectory length, denoted as t, between samples. Alternatively, one can adjust the trajectory length to be shorter, reaching a point at which the HMD algorithm closely resembles the original Langevin algorithm. In this study, we adopt a method that combines elements of both approaches.

Algorithm 1: HMD algorithm for NSPT

Step 1: Set $U^{(1)} = I$,$U^{(k)} = P^{(k)} = 0$ for $k = 2$·

Step 2: Generate $P^{(1)}$ with Gaussian distribution as

$$P^{(1)} = \sum_{k=1}^{N^2-1} \eta^k T^k \tag{44}$$

$$\eta \in \textbf{Normal}(0, \sqrt{2}) \tag{45}$$

$$\mathrm{Tr}\left[T^\alpha T^\beta\right] = \frac{\delta_{\alpha,\beta}}{2} \tag{46}$$

where T^k are in $SU(N)$ Lie-algebra

Step 3: Randomize the fictitious times

$$\begin{aligned} N &\in \text{Binomial}(N_{md} - 1, 0.5) + 1 \\ t &= N\delta t \end{aligned} \tag{47}$$

Step 4: Integrate the EoM numerically for the t derived from the third step.

Step 5: Calculate observable and back to step 2

For the symplectic integrator in (38) and (39), we utilize the 4th-order Omelyan-Mryglod-Folk (OMF) integrator as described in Refs. [61, 65]. This integrator is expected to introduce finite integration errors proportional to δt^4.

The randomized trajectory length by which the ergodicty of the evolution is improved, denoted as t_r, is determined by:

$$t_r = n_r \delta t, \quad \delta t = t/N_{md}, \tag{48}$$

where t represents a fixed length of trajectory, N_{md} is an integer representing the number of time steps, and n_r is a random number with the binomial distribution $n_r \leftarrow B(1/2, 2(N_{md} - 1)) + 1$, using the binomial distribution $B(p, n)$. Consequently, the mean value of trajectory length is $\langle t_r \rangle =$

t. All numerical results are computed at various N_{md} values and extrapolated to $N_{md} \to \infty$ following the δt^4 scaling before analyzing the N dependence.

The equation of motion evolves for the randomized trajectory length, and the stochastic variables $U^{(k)}, k = 1, \ldots$, representing perturbative coefficients, are sampled as the Monte Carlo ensemble. The observable is also perturbatively expanded in terms of λ, where the perturbative coefficients are functions of $U^{(k)}, k = 1, \ldots$. The detailed algorithms for implementing NSPT in TRPCM, including the randomized trajectory length, can be found in Algorithm 1.

The internal energy density operator E in Eq. (16) is expanded as follows:

$$E = \sum_{k=0}^{\infty} \lambda^{k/2} E^{(k)}, \tag{49}$$

$$E^{(k)} = \frac{1}{2N} \sum_{\mu} \mathrm{Re}\,\mathrm{Tr} \left[\left(U\Gamma_\mu \circledast U^\dagger \Gamma_\mu^\dagger \right)^{(k)} \right]. \tag{50}$$

The expectation value of the coefficient, $\left\langle E^{(k)} \right\rangle$, is calculated as the statistical average within the ensemble of $U^{(k)}, k = 1, \ldots$. The perturbation series is truncated to a fixed order in the actual numerical simulation. In this thesis, we will introduce two types of simulation using different set of truncated order and N. More details, concerning the numerical simulation for achieving both large N limit and high-order, will be argued in the next section.

3.3 Paterson-Stockmeyer method for matrix exponential

This subsection is based on our recent work and more details can be found in Ref. [62]. The purpose of this subsection is to optimize HMD-based NSPT to achieve improved performance, particularly for high-order calculations. To accomplish this, the initial step involves identifying the most computationally intensive segment within the NSPT algorithm. Based on our estimation, this lies in the computation of the matrix exponential appeard in Eq. (38).

We begin by introducing the concept of the matrix exponential. The input matrix, denoted as

A, is expressed through expansion as follows:

$$EXP = \exp(iA), \quad A = \sum_{j=1}^{N_{\text{PT}}} g^j A^{(j)}, \tag{51}$$

where N_{PT} represents the upper limit of the expansion order, and g is a coupling constant. The matrix exponential of A is formally defined as:

$$EXP = \exp\left(i \sum_{j=1}^{N_{\text{PT}}} g^j A^{(j)} \right). \tag{52}$$

In the framework of the NSPT formalism, our aim is to compute the perturbative series of EXP, which emerges in Eq. (38), as illustrated by:

$$EXP = \sum_{j=0}^{N_{\text{PT}}} g^j EXP^{(j)}, \tag{53}$$

where the initial term is $EXP^{(0)} = I$ (the identity matrix). The perturbation coefficient matrix $EXP^{(k)}$ is a function of $A^{(j)}$ for $j = 1, 2 \ldots, N_{\text{PT}}$. The functional form can be evaluated by expanding Eq. (52) in terms of g;

$$EXP = I + \sum_{j=1}^{N_{\text{PT}}} g^j EXP^{(j)} = \exp\left(i \sum_{k=1}^{N_{\text{PT}}} g^k A^{(k)} \right) = \sum_{j=0}^{N_{\text{PT}}} \frac{(i)^j}{j!} \left[\sum_{k=1}^{N_{\text{PT}}} g^k A^{(k)} \right]^j. \tag{54}$$

We combine the Taylor series expansion of the matrix exponential with the coupling constant expansion of the input matrix. Through the expansion of this double series, we obtain an initial expression for each $EXP^{(k)}$ as a function of $A^{(k)}$ for $k = 1, 2, \ldots, N_{\text{PT}}$.

Various algorithms are available for calculating the matrix exponential. However, within the NSPT framework, managing the intricate double expansion relationships presents a significant challenge. To address this complexity, we introduce Horner's method as an approach. The trun-

cated form of Eq. (54) can be computed using the following expression:

$$\begin{aligned} EXP &= I + c_1 A + c_2 A^2 + c_3 A^3 + \cdots + c_{N_{\rm PT}} A^{N_{\rm PT}} \\ &= I + c_1 A \left(I + \frac{c_2}{c_1} A \left(I + \frac{c_3}{c_2} A \left(I + \cdots + \frac{c_{N_{\rm PT}-1}}{c_{N_{\rm PT}-2}} A \left(I + \frac{c_{N_{\rm PT}}}{c_{N_{\rm PT}-1}} A \right) \cdots \right) \right) \right). \end{aligned} \tag{55}$$

In the equation above, $c_j = \frac{i^j}{j!}$. It is important to note that in the NSPT context, all operations involving powers and matrix multiplications are executed in terms of perturbative convolution of Eq. (41). The first line of Eq. (55) represents the naive approach to compute the truncated matrix exponential, where the number of matrix-matrix multiplications of A is $(N_{\rm PT}(N_{\rm PT}+1)/2)$, which is of the order of $\mathcal{O}(N_{\rm PT}^2)$ for the non-perturbative case. The NSPT version replaces all matrix-matrix multiplications with convolution operations using the coupling constant expansion of A, incurring a cost of $\mathcal{O}(N_{\rm PT}^2)$ for the naive convolution algorithm. Consequently, the total computational complexity of the naive matrix exponential method in NSPT is $\mathcal{O}(N_{\rm PT}^4)$. On the other hand, the second line demonstrates the application of Horner's method, which significantly reduces the computational complexity to $\mathcal{O}(N_{\rm PT}^3)$.

Since our goal in this study is to explore the high-order perturbative behavior of TRPCM and extract information about the existence of renormalons, a reasonable choice for $N_{\rm PT}$ is around $\mathcal{O}(100)$. However, this presents a significant computational challenge. Although Horner's method reduces the computational complexity from $\mathcal{O}(N_{\rm PT}^4)$ to $\mathcal{O}(N_{\rm PT}^3)$, a faster algorithm would greatly benefit our numerical simulations, and we will show the algorithm we recently employed called Paterson-Stockmeyer (P-S) method.

Efficient polynomial evaluations involving matrices can be achieved through the P-S algorithm. Current research efforts focus on further enhancing and refining this method within the academic literature [66, 67, 68].

We initially present the P-S algorithm as applied to the truncated Taylor series described in Eq. (54). Subsequently, we extend this methodology to encompass the NSPT variant, where the input matrix itself takes the form of a perturbation series. Anticipated benefits include a reduction in the number of matrix-matrix multiplications when evaluating the truncated Taylor series of the matrix exponential or, equivalently, a matrix polynomial. This effectively reduces the computational

overhead associated with convolution operations within the NSPT framework.

To streamline the computational process, we commence by partitioning the N_{PT} terms within the polynomial into groups. Each group consists of a matrix polynomial containing either s, δ, or v terms.

$$
\begin{aligned}
EXP &\simeq \exp\left[iA\right] \\
&= I + iA + \frac{(i)^2}{2!}A^2 + \frac{(i)^3}{3!}A^3 + \frac{(i)^4}{4!}A^4 + \cdots + \frac{(i)^{N_{\text{PT}}-1}}{(N_{\text{PT}}-1)!}A^{N_{\text{PT}}-1} + \frac{(i)^{N_{\text{PT}}}}{N_{\text{PT}}!}A^{N_{\text{PT}}} \\
&= I + iA + \frac{(i)^2}{2!}A^2 + \cdots + \frac{(i)^{s-1}}{(s-1)!}A^{s-1} \\
&+ \frac{(i)^s}{s!}A^s\left[I + \frac{i(s!)}{(s+1)!}A + \frac{(i)^2(s!)}{(s+2)!}A^2 + \cdots + \frac{(i)^{s-1}(s!)}{(2s-1)!}A^{s-1}\right] \\
&+ \frac{(i)^{2s}}{(2s)!}A^{2s}\left[I + \frac{i(2s)!}{(2s+1)!}A + \frac{(i)^2(2s)!}{(2s+2)!}A^2 + \cdots + \frac{(i)^{s-1}(2s)!}{(3s-1)!}A^{s-1}\right] + \cdots \\
&+ \frac{(i)^{vs}}{(vs)!}A^{vs}\left[I + \frac{i(vs)!}{(vs+1)!}A + \frac{(i)^2(vs)!}{(vs+2)!}A^2 + \cdots + \frac{(i)^{N_{\text{PT}}-vs}(vs)!}{N_{\text{PT}}!}A^{N_{\text{PT}}-vs}\right] \\
&= Q_0 + A^s\left[Q_1 + A^s\left[Q_2 + \cdots + A^s\left[Q_{v-1} + A^s Q_v\right]\ldots\right]\right],
\end{aligned}
\tag{56}
$$

where $N_{\text{PT}} = sv + \delta$, with δ defined as the integer remainder when dividing N_{PT} by s. We also define:

$$
Q_v = \sum_{k=0}^{\delta} c_{sv+k}A^k, \quad Q_i = \sum_{k=0}^{s-1} c_{si+k}A^k, \quad i = 0, 1, \ldots, v-1. \tag{57}
$$

Upon reorganization, it becomes evident that the powers of the matrix A appear repeatedly during the computations in Eq. (56). With this observation in mind, if we can pre-compute these matrix powers A^k and reuse them throughout the entire computation of Q_j and Q_v, we can anticipate a significant improvement in computational efficiency. This form contains three hyperparameters (s, v, δ) that have not yet been determined. These parameters can be varied to optimize the total count of matrix-matrix multiplications. To identify the optimal choices, we can establish the

following relations, ignoring the remainder part δ,

$$N_{\text{PT}} = sv, \tag{58}$$

$$N_{\text{Op}} = s - 2 + 1 + v, \tag{59}$$

where N_{Op} represents the total number of matrix-matrix multiplications in Eq. (56). The minimum value for N_{Op} is achieved when $s = \sqrt{N_{\text{PT}}}$ for a large constant N_{PT}, and the optimal N_{Op} is $N_{\text{Op}} = 2\sqrt{N_{\text{PT}}}$. For non-zero δ, the optimal choice has been determined as [67]:

$$s = \text{Floor}\left(\sqrt{N_{\text{PT}}}\right), \tag{60}$$

$$v \equiv \left\lfloor \frac{N_{\text{PT}}}{s} \right\rfloor = \text{Floor}\left(\frac{N_{\text{PT}}}{s}\right). \tag{61}$$

To evaluate the computational cost of the P-S method within NSPT, it is important to note that all matrix-matrix multiplications are replaced by convolution operations in terms of the coupling constant expansion. In a convolution operation for the perturbation series truncated at N_{PT}, the number of matrix-matrix multiplications is N_{PT}^2 with the naive convolution operation. However, with the P-S method, the optimal number of matrix-matrix multiplications is approximately $2\sqrt{N_{\text{PT}}} \times N_{\text{PT}}^2$, which scales as $\mathcal{O}(N_{\text{PT}}^{5/2})$. The expected improvement factor of the P-S method over Horner's method is $\mathcal{O}(N_{\text{PT}}^{-0.5})$, and we will verify this in the following section. Additional details and pseudo-code related to the P-S method is located in Algorithm 2 and Ref. [62].

In this section, we introduced NSPT and demonstrated how to integrate NSPT with TRPCM. NSPT is a powerful tool that allows us to achieve high-order perturbative behavior, which traditional Feynman diagram-based methods struggle with. Utilizing NSPT enables us to investigate the renormalon behavior directly. Despite the advantages NSPT provides, it remains computationally intensive, particularly when aiming for very high-order calculations, such as $N_{\text{PT}} = \mathcal{O}(100)$. To address this challenge, we presented a new algorithm, the P-S method as above. This method effectively reduces computational costs, enabling us to reach high-order calculations. I will show more details about the efficiency of this algorithm in the following section, which is based on our work in Ref. [62].

Algorithm 2: Paterson-Stockmeyer algorithm for matrix exponential for NSPT

1:$s = \mathrm{Floor}(\sqrt{N}); v = \mathrm{Floor}(N/s); \delta = \mathrm{mod}(N, s)$

2: $P_1^{(p)} := p^{(p)}$ (for $p = 0, \ldots, N_{\text{urunc}}$)

3: for $k = 2, \ldots, s$ do

4: $P_k^{(p)} := (P_1 * P_{k-1})^{(p)}$ (for $p = 0, \ldots, N_{\text{trunc}}$)

5: end for

6: for $j = 0, \ldots, v$ do

7: if $j < v$ then

8: $i_{\max} = s - 1$

9: else if $j == v \&\& \delta \neq 0$ then

10: $i_{\max} = \delta$

11:end if

12: if $i_{\max} \neq 0$ then

13: $\tilde{Q}_j^{(p)} := \frac{c_{sj+i_{\max}}}{c_{sj+i_{\max}-1}} P_{i_{\max}}^{(p)}$ (for $p = 0, \ldots, N_{\text{trusc}}$)

14: for $i = i_{\max} - 1, 1, -1$ do

15: $Q_j^{(p)} := \frac{c_{sj+i}}{c_{sj+i-1}} \left(P_i^{(p)} + Q_j^{(p)} \right)$ (for $p = 0, \ldots, N_{\text{trunc}}$)

16: end for

17: $\tilde{Q}_j^{(0)} := I + \tilde{Q}_j^{(0)}$

18: end if

19: end for

20: if $\delta == 0$ then

21: $E^{(p)} = \tilde{Q}_{v-1}^{(p)} + \frac{c_{sv}}{c_{sv-s}} P_s^{(p)}$ (for $p = 0, \ldots, N_{\text{urunc}}$)

22: else

23: $E^{(p)} = \tilde{Q}_{v-1}^{(p)} + \frac{c_{sv}}{c_{sv-s}} \left(P_s * \tilde{Q}_v \right)^{(p)}$ (for $p = 0, \ldots, N_{\text{trunc}}$)

24: end if

25: for $j = v - 2, 0, -1$ do

26: $E^{(p)} = \tilde{Q}_j^{(p)} + \frac{c_{sj+s}}{c_{sj}} (P_s * E)^{(p)}$ (for $p = 0, \ldots, N_{\text{trunc}}$)

27: end for

4 Numerical results

In this section, we present our numerical results for the study of TRPCM using NSPT. In Section 4.1, we provide details about the hyperparameters of the model and the HMD used in the simulation. In Section 4.2, we present the large N results at the λ^4 level and compare them to the PCM in infinite volume. Large N field theories and matrix models exhibit an important property known as large N factorization. Numerically demonstrating the existence of large N factorization is crucial, especially when considering error estimates and the concept of a "single simulation." Our primary goal is to investigate the high-order behavior and detect the signal of renormalons. However, high-order calculations are time-consuming. We conducted a micro-benchmark to identify the most computationally intensive part of the simulation, which led to the optimization of the matrix exponential calculation using the newly developed P-S method introduced in Section 3.3. In Section 4.3, we demonstrate the efficiency of the P-S method compared to Horner's method. In the final subsection, using the newly developed P-S method, we calculate the high-order perturbative coefficients of the internal energy and provide evidence of renormalons.

The numerical simulation in Section 4.2 is based on our work in Ref.[69], while Section4.3 is grounded in our work detailed in Ref.[62]. Finally, Section4.4, which primarily presents the high-order behavior of TRPCM using the P-S method, was discussed at the 78th Annual Meeting of the Physical Society of Japan (JPS) [70].

4.1 Numerical setup

The NSPT simulation is a powerful tool for handling perturbative calculations in TRPCM. As two key hyperparameters, namely N and N_{PT}, are set to significantly large values, the simulation becomes computationally intensive. In each of the following subsections, specific objectives are pursued. Therefore, selecting appropriate hyperparameters is crucial to ensure that the simulation can be completed efficiently while serving its intended purpose.

In Section 4.2, our objective is to show that results for large N can be obtained using an extrapolation method. To achieve this, we fix $N_{PT} = 4$ in the 't Hooft coupling expansion and

select values for N ranging from small to intermediate. The flux parameter k for each choice of N is determined using Eq.(13). Additional details are available in Table1. These parameters are chosen to explore the large N factorization and statistical error of the perturbation coefficients, aiming to validate whether the concept of a single simulation holds for a sufficiently large N.

N	$(\frac{L}{a})^2$	K	$\bar{K}$	$\frac{\bar{K}}{N}$	N_{md}	**Statistics**
					10	10 000 000
3	9	1	1	0.33	12	10 000 000
					20	10 000 000
					10	10 000 000
5	25	3	2	0.4	12	10 000 000
					20	10 000 000
					10	10 000 000
7	49	5	3	0.43	12	10 000 000
					20	10 000 000
					10	10 000 000
9	81	7	4	0.44	12	10 000 000
					20	10 000 000
					10	10 000 000
11	121	3	4	0.36	12	10 000 000
					20	10 000 000
					10	10 000 000
13	169	8	5	0.38	12	10 000 000
					20	10 000 000
					10	10 000 000
15	225	4	4	0.27	12	11 000 000
					20	10 000 000
					10	7 240 200
17	289	5	6	0.35	12	7 944 400

					20	4 684 000
					10	9 000 000
19	361	11	7	0.37	12	8 435 100
					20	6 435 800
					10	2 036 200
21	441	8	8	0.38	12	3 084 400
					20	2 411 300

Table 1: Simulation parameter for Section 4.2.

In Section 4.3, our aim is to demonstrate the computational efficiency of the P-S method. For this purpose, we choose an intermediate value for $N = 17, 55$ that does not significantly sacrifice program execution time, and we vary $N_{PT} = 10, 20, 40, 100, 200, 500, 1000$. This range is suitable for establishing the presence of renormalons.

In the final subsection, we aim to confirm the existence of renormalons through both large N and high-order results. To do so, we set $N_{PT} = 20$ in the 't Hooft coupling expansion, and the choice of (N, K) pairs is based on the Fibonacci series in Eq. (15). The choice of setting $N_{PT} = 20$ remains consistent with the work in Ref. [46], which has shown that for small choice N $N_{PT} = 20$ is large enough to extract the signal of renormalons. Therefore, we have the same choice .Further information regarding the statistics can be found in Table. 2

(N, K)	Statistics
55,21	51
89,34	50
144,55	37
233,89	30

Table 2: Simulation parameter for Section 4.4.

Apart from the hyperparameter choices for TRPCM, we also need to consider other hyperparameters in the HMD-based NSPT simulation. The trajectory length t and the number of trajectory

time steps N_{md} need to be fine-tuned to satisfy the large N factorization property, which means that the variance of the perturbative coefficients diminishes in the large N limit. In summary, we've found that a trajectory length of $t = 0.05$ is sufficient for achieving large N factorization for the first four-order coefficients, and we can use this choice in all the simulations mentioned above.

In contrast to non-perturbative simulations using Hybrid Monte Carlo, in the NSPT case, there is no Metropolis test to eliminate the systematic error arising from finite size effects in discretized fictitious time integration. For each value of N, we run the simulation with different settings, such as $N_{md} = 10, 12, 20$, and evaluate results without discretized errors using extrapolation. Additionally, to mitigate autocorrelation among the samples, we sample every trajectory and group every 100 trajectories into a bin. The statistical errors are estimated by Jackknife method.

For our numerical study, we utilized the subsystem A within the ITO supercomputer [71] at Kyushu University. To fully leverage the available hardware resources, we employed the OpenMP framework to parallelize both the program based on Horner's method and the one based on the P-S method. Additionally, for efficient matrix-matrix multiplication operations, we utilized the ZGEMM function from the MKL library, provided by Intel. The version of the compiler, Intel Fortran, is $19.0.4.243$.

It's noteworthy that the performance of ZGEMM decreases as the size of the matrix N decreases to a certain extent [72], particularly when N is smaller than 1000. In TRPCM or other matrix-valued field theory cases where the problem size typically ranges from 100 to 1000, the overhead incurred by multiple invocations of the ZGEMM function becomes noticeably substantial. To address this issue, in Section 4.3 and 4.4, we employed the ZGEMM-BATCH subroutine, effectively alleviating the overhead associated with frequent function calls. However, for the results presented in Section4.2, we implemented the ZGEMM subroutine from MKL.

4.2 Large N results with extrapolation: large N factorization and estimation of error

In the large N limit, the first three-order results can be compared with the analytic ones of the PCM on an infinite-volume lattice. More detailed results are available in Refs. [73, 74]. However,

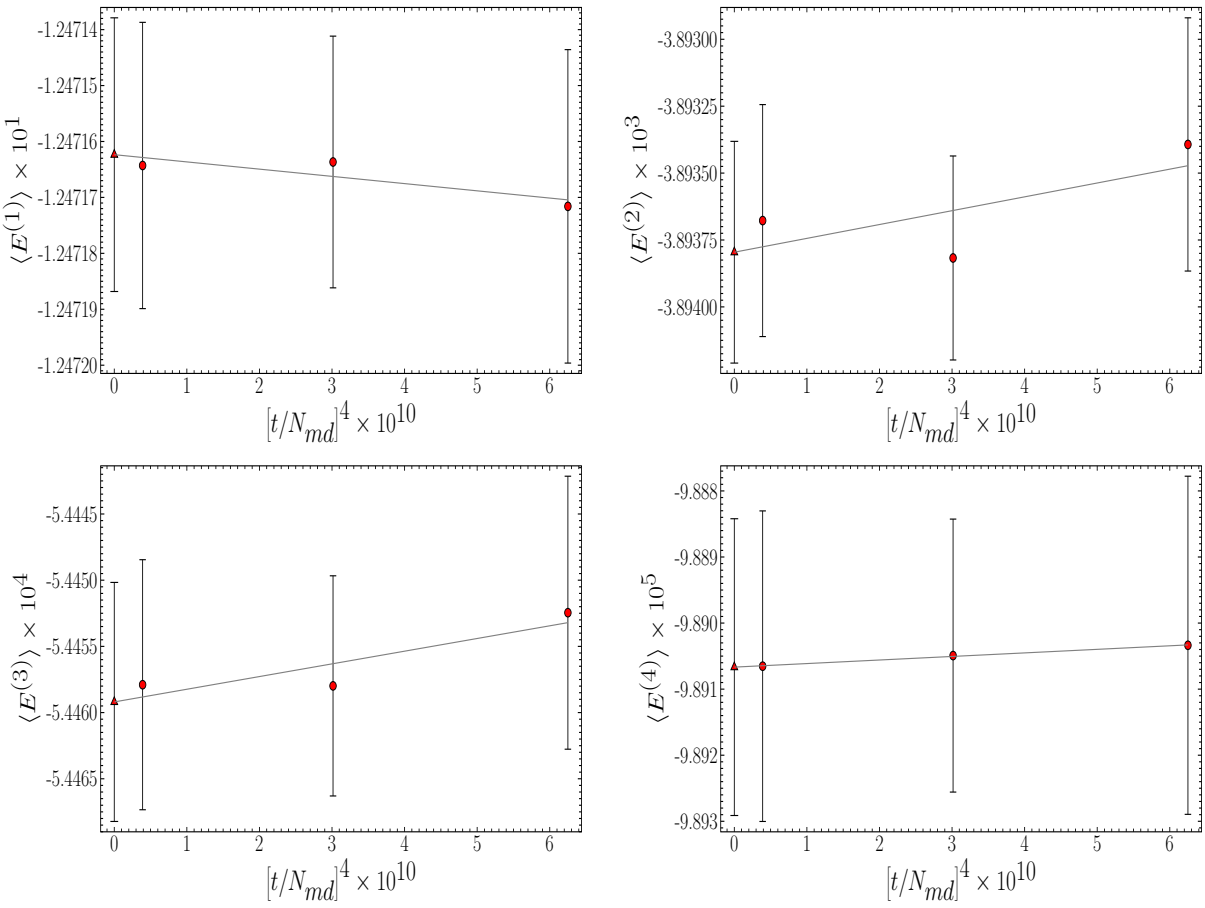

Figure 1: This figure provides an overview of the extrapolation process towards the vanishing MD step size, where $\left[\frac{t}{N_{md}}\right]^4 = \delta t^4 \to 0$. The figure displays our numerical results, which were obtained from $N = 21$ up to the fourth order. To determine the perturbative coefficients at $\delta t = 0$, a linear fitting procedure is employed by regressing the data against $\left[\frac{t}{N_{md}}\right]^4$.

as the analytic formula for the fourth-order coefficient of PCM is absent, a direct comparison of the fourth-order coefficients between the TRPCM case and the PCM case is not feasible. To gain insight into the behavior of $\left\langle E^{(4)} \right\rangle$ in the large N limit, we turn to the results from NSPT simulations of PCM conducted by Bruckmann and Puhr [46], with raw data available in Ref. [75]. Additionally, because their results are limited to smaller N, we, therefore, performed a separate NSPT simulation for PCM with various volumes and extrapolated the results to infinite volume. A detailed account of our NSPT simulation of PCM is provided in our main work's paper [69]

In Fig. 1, we present an illustrative example of the extrapolation to a vanishing MD step

N	$\langle E^{(1)} \rangle$	$\langle E^{(2)} \rangle$	$\langle E^{(3)} \rangle$	$\langle E^{(4)} \rangle$
3	-0.11112234(1477)	-0.00328153(185)	-0.00049017(43)	-0.00010100(13)
5	-0.12000053(808)	-0.00367717(110)	-0.00052990(23)	-0.00010180(6)
7	-0.12245450(527)	-0.00379498(75)	-0.00054004(16)	-0.00010128(4)
9	-0.12345411(379)	-0.00384602(56)	-0.00054238(12)	-0.00010108(3)
11	-0.12396632(289)	-0.00386240(44)	-0.00054371(9)	-0.00009996(2)
13	-0.12425785(230)	-0.00387216(36)	-0.00054340(8)	-0.00009976(2)
15	-0.12444483(188)	-0.00388285(30)	-0.00054445(6)	-0.00009937(2)
17	-0.12456844(226)	-0.00388773(37)	-0.00054450(8)	-0.00009915(2)
19	-0.12465177(166)	-0.00389026(28)	-0.00054433(6)	-0.00009896(1)
21	-0.12471624(245)	-0.00389380(41)	-0.00054459(9)	-0.00009891(2)

Table 3: Perturbative coefficients for the internal energy were obtained by extrapolating to vanishing integration step size

size for the internal energy up to the fourth order, specifically for $N = 21$. To achieve this, we utilized a 4th-order OMF integrator and performed a linear extrapolation with respect to δt^4. This linear dependence was consistently observed for other values of N under investigation, effectively mitigating the systematic errors arising from the finite fictitious time step size. Consequently, the numerical results we employ for further discussions are obtained at a vanishing MD step size and are free from the systematic error.

The perturbative coefficients of the internal energy at vanishing MD step size for various values of N are provided in Table 3. Figure 2 depicts the N dependence of perturbative coefficients of the internal energy up to the fourth order. The red dots represent the results obtained using TR-PCM with NSPT, while the solid curves correspond to the analytic formula referenced in Ref.[73] for PCM on an infinite volume lattice. We also list the first three order analytic expressions for the PCM coefficients in an infinite volume, which are:

$$\langle E^{(1)} \rangle = -\frac{N^2-1}{8N^2}, \tag{62}$$

$$\langle E^{(2)} \rangle = -\frac{N^2-1}{8N^2} \times \frac{N^2-2}{32N^2}, \tag{63}$$

$$\langle E^{(3)} \rangle = -\frac{N^2-1}{8N^2}\left[\frac{3N^4-14N^2+20}{768N^4} + \frac{N^4-4N^2+12}{64N^4}Q_1 + \frac{N^4-8N^2+24}{64N^4}Q_2\right], \tag{64}$$

where $Q_1 = 0.0958876$ and $Q_2 = -0.0670$ [73]. In the appendix of our primary work [69] in

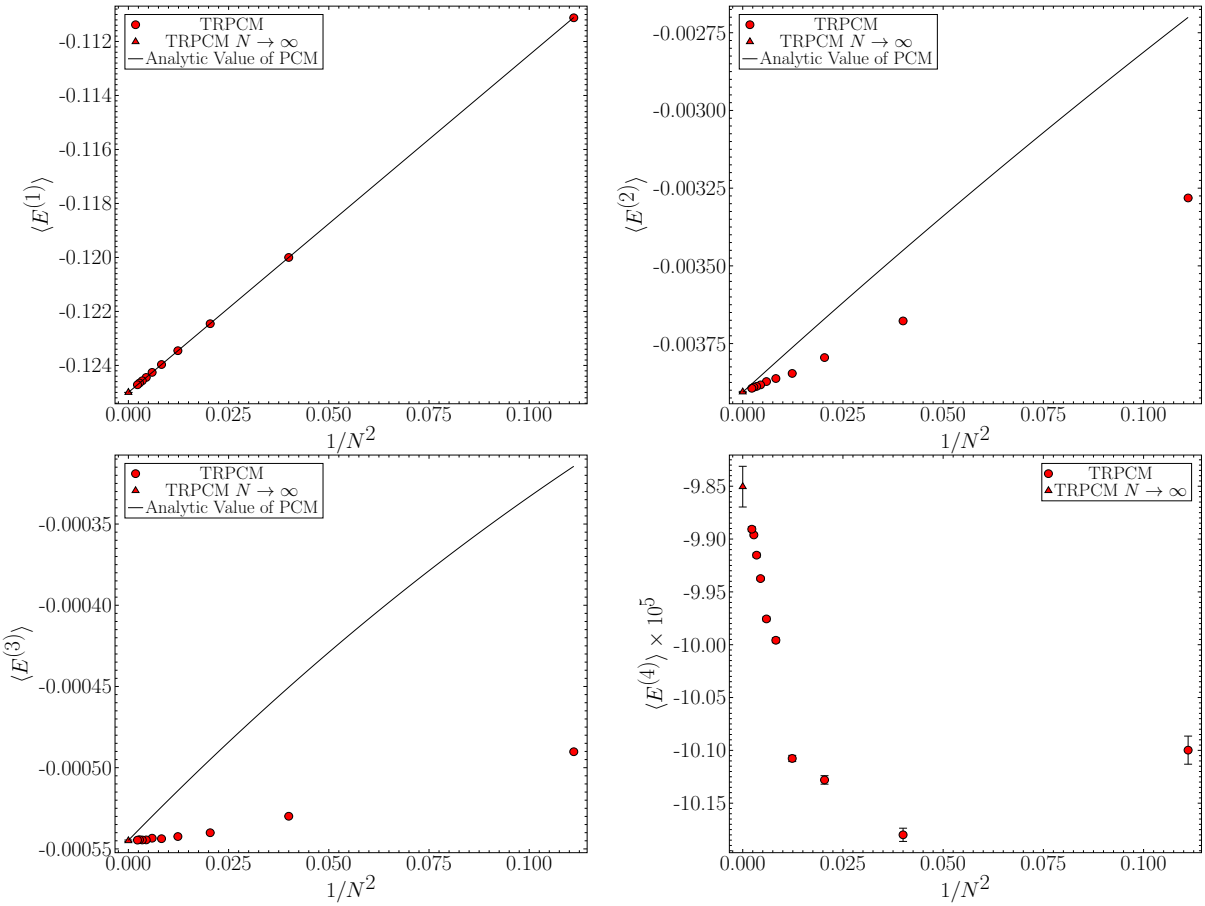

Figure 2: These figures display the dependence of perturbative coefficients of the internal energy on the parameter N up to the fourth order. Solid lines are plotted to represent the equations from Eq.(80) to Eq.(64) as a function of $1/N^2$.

which we have provided the analytic equations for the second-order coefficient of the TRPCM concerning our specific values of N and K and a comparison between the numerical and analytic results can be found. This inclusion demonstrates the complete consistency of the results obtained through NSPT with these analytical values.

As observed in Fig. 2, the leading-order results ($E^{(1)}$) coincide with those of the PCM, while discrepancies arise for the second and third-order coefficients at finite N. Notably, the N dependence of the TRPCM exhibits a milder slope compared to that of PCM, suggesting that the large N limit can be efficiently approached using TRPCM. This effectiveness is further enhanced by the reduced N dependence compared to PCM, where it is necessary to simulate the model with

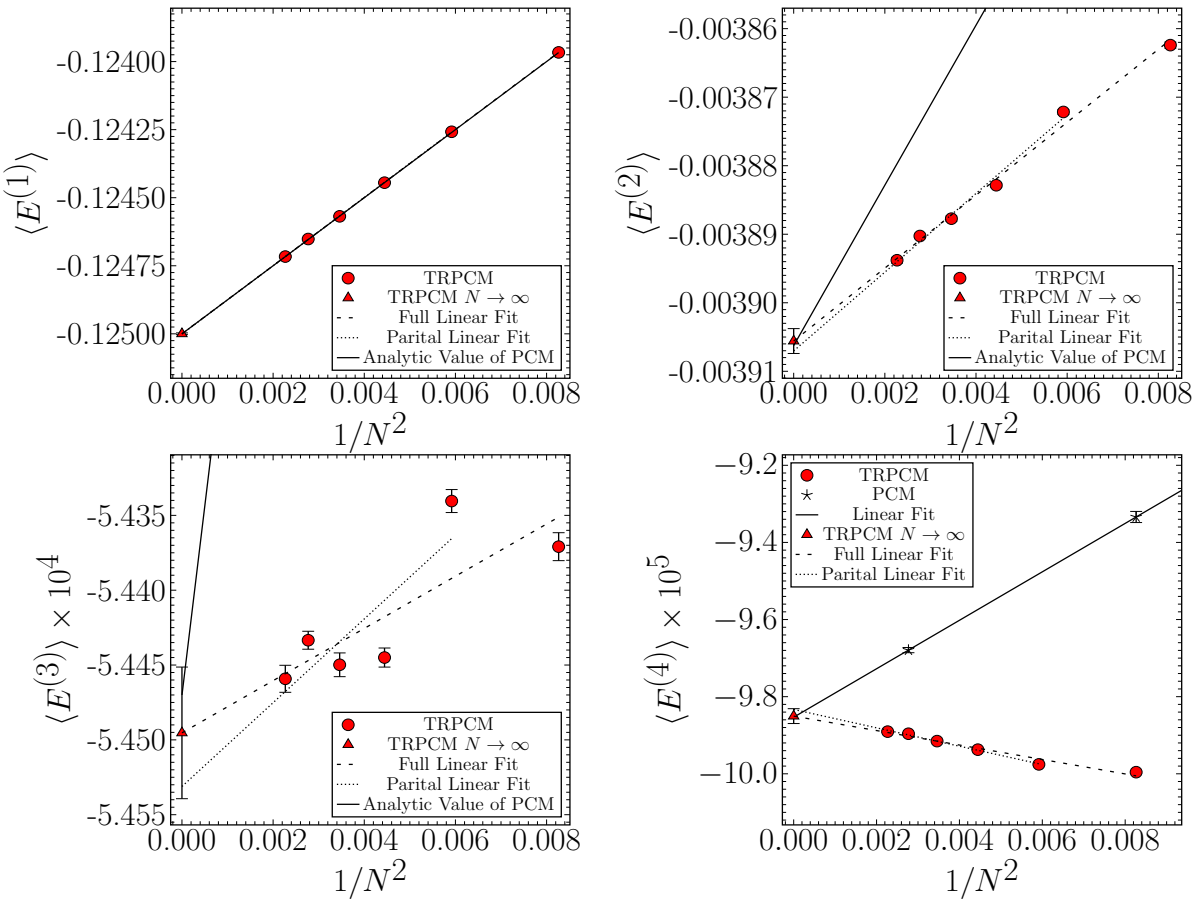

Figure 3: These figures provide a close-up view of the data presented in Fig. 2, focusing on the limits as N approaches infinity.

different volumes and N.

In the TRPCM, the N dependence encompasses both finite N and finite volume corrections. We conducted linear fits on NSPT data in terms of $1/N^2$, and the dashed and dotted lines in Fig. 3 represent the fitting results. Our focus on the leading finite N correction entails fitting the data with $N \geq 11$. The dashed and dotted lines illustrate the fit for $N \geq 11$ and the fit excluding $N \leq 11$, respectively. The red triangle at $1/N^2 \to 0$ corresponds to the large N extrapolation. The central value is based on the dashed fit, and the error bar accounts for both statistical and systematic errors. The difference between two fittings is used to estimate the systematic error for the extrapolation.

Table 4 presents the large N limit of the first four coefficients of the internal energy for the TRPCM. The first three coefficients are consistent with the analytic results of the PCM in the large

Order i of $\langle E^{(i)} \rangle$	Analytic	NSPT
1	-0.125	-0.12499981(234)(83)
2	-0.00390625	-0.00390558(38)(143)
3	-0.00054470	-0.000544953(82)(358)
4	N.A.	-0.000098504(20)(172)

Table 4: Comparison between analytic and NSPT results for $N \to \infty$. The first error corresponds to the statistical error, while the second error arises from the systematic errors in the fitting range.

N limit. For the fourth-order coefficient, additional calculations were performed involving perturbative coefficients of the PCM at $N = 11$ and 19 for various volumes. These coefficients were then used to perform the infinite volume limit (for details, refer to [69]). The 2-point extrapolation of the PCM data aligns with that of the TRPCM in the large N limit. It is worth noting that the slope of the TRPCM is still smaller than that of the PCM, indicating a smaller finite N correction. The TRPCM is thus more efficient in reaching the large N limit than the PCM.

Beyond the leading order, finite N corrections become apparent [76]. The linear fitting results obtained using $N \geq 11$ are as follows

$$\langle E^{(1)} \rangle = -0.12499981(248) + \frac{0.12510(52)}{N^2}, \tag{65}$$

$$\langle E^{(2)} \rangle = -0.00390558(147) + \frac{0.005320(82)}{N^2}, \tag{66}$$

$$\langle E^{(3)} \rangle = -0.000544953(367) + \frac{0.000174(17)}{N^2}, \tag{67}$$

$$\langle E^{(4)} \rangle = -0.000098504(173) + \frac{-0.0001874(42)}{N^2}. \tag{68}$$

The coefficients of the $\mathcal{O}(1/N^2)$ term for $\langle E^{(2)} \rangle$ and $\langle E^{(3)} \rangle$ are smaller than those of PCM (approximately $3/256 \approx 0.01771875$ for $\langle E^{(2)} \rangle$ and 0.002525595 for $\langle E^{(3)} \rangle$).

Our results also suggest that the magnitude of the coefficient for the $1/N^2$ term is of the same order as that of the constant term for each order. This observation enables us to further discuss the idea of a single simulation. In this study, our goal is to evaluate coefficients at both high-order and the large N limit. The concept of a single simulation, which aligns with the philosophy of master field first presented by Witten [77], involves conducting a single simulation at a finite but sufficiently large N value. This approach allows us to treat the results from finite N as if they

were obtained in the infinite N limit. How to determine specific N value is based on the condition that the magnitude of the finite N correction is smaller than the statistical error, ensuring reliable results. At this point, the large N factorization property enters the game because the factorization directly correlates with the statistical error.

In accordance with large N factorization, the expectation value of the product of single-trace local operators at distinct lattice sites becomes the product of the individual expectation values of the local operators plus some finite N correction which decreases as a function of $f(1/N)$. As taking the $N = \infty$ limit, the two local operators become independent. This property is crucial to the single simulation and can be verifiable by examining the statistical variance of a local operator in the TRPCM for example the internal energy.

On the other hand, the statistical error is directly linked to the variance and the number of independent samples obtained from MCMC. Taking the large N factorization into account, it results in a decrease in variance as N increases. This implies a reduced requirement for the number of independent samples needed to achieve a specific level of precision with NSPT for the perturbative coefficients of the internal energy. A similar phenomenon occurs in the duality between classical physics and quantum physics. As the Planck constant h approaches zero, fluctuations vanish, and classical physics can be viewed as a classical approach to quantum physics.

The factorization property shows that the variance of the internal energy, $\mathrm{Var}\,[E]$, as $N \to \infty$ should behave

$$\mathrm{Var}\,[E] = \left\langle E^2 \right\rangle - \langle E \rangle^2 \quad \underset{N\to\infty}{\to} \quad 0. \tag{69}$$

To ascertain whether the large N factorization occurs in the numerical simulation, we compute the variance for the perturbation coefficient obtained from NSPT at each order.

Figure 4 and Table 5 illustrate the dependence of the variance on N. Figure 5 zooms in on the behavior at the large N limit. The variance is still fitted using a linear function of $1/N^2$, as follows:

N	$\mathrm{Var}[E^{(1)}]\times 10^4$	$\mathrm{Var}[E^{(2)}]\times 10^6$	$\mathrm{Var}[E^{(3)}]\times 10^7$	$\mathrm{Var}[E^{(4)}]\times 10^8$
3	0.2312(10)	0.3639(17)	0.1941(12)	0.1874(19)
5	0.06919(30)	0.12763(56)	0.05845(27)	0.04153(22)
7	0.02938(12)	0.06003(26)	0.02670(11)	0.017085(79)
9	0.015236(66)	0.03374(14)	0.014971(65)	0.009203(41)
11	0.008863(38)	0.020659(90)	0.009228(40)	0.005554(24)
13	0.005601(24)	0.013890(61)	0.006247(27)	0.003741(17)
15	0.003789(16)	0.009662(42)	0.004364(18)	0.002578(11)
17	0.002705(14)	0.007339(39)	0.003375(18)	0.002047(11)
19	0.001981(95)	0.005496(26)	0.002575(12)	0.0015712(75)
21	0.001510(12)	0.004325(33)	0.002064(15)	0.0012717(99)

Table 5: Variance of the perturbative coefficients for the internal energy after extrapolation to a vanishing integration step size.

Order i of $\mathrm{Var}[E^{(i)}]$	$\mathrm{Var}[E^{(i)}]_{N\to\infty}$	$a^{(i)}$
1	-0.786(45)(834)$\times 10^{-7}$	0.11242(68)$\times 10^{-3}$
2	-0.119(11)(111)$\times 10^{-8}$	0.2612(17)$\times 10^{-5}$
3	-0.403(54)(440)$\times 10^{-10}$	0.11403(78)$\times 10^{-6}$
4	-0.198(33)(282)$\times 10^{-11}$	0.6693(47)$\times 10^{-8}$

Table 6: Variance of the internal energy after extrapolating to infinite N

$$\mathrm{Var}(E^{(k)}) = \mathrm{Var}(E^{(k)})_{N\to\infty} + \frac{a^{(k)}}{N^2}. \tag{70}$$

The dashed and dotted lines represent the fitting results with $N \geq 11$ and with $N \geq 13$ data, respectively. It is evident that the variance approaches zero in the limit as N tends to infinity. The red triangles at $N = \infty$ correspond to the results obtained without $N = 11$ data, and the error bars include both statistical and systematic errors, calculated from the two fitting results. The large N results are presented in Table 6, where the first and second errors denote the statistical and systematic errors, respectively, and the fitting results for $\mathrm{Var}(E^{(k)})_{N\to\infty}$ are nearly zero when considering the error, which demonstrates the effectiveness of our simulation setup in preserving the large N factorization.

These findings serve as a robust cross-check for the reliability of our NSPT results up to the fourth order. Additionally, it is noteworthy that as the order k increases, the slope $a^{(k)}$ decreases.

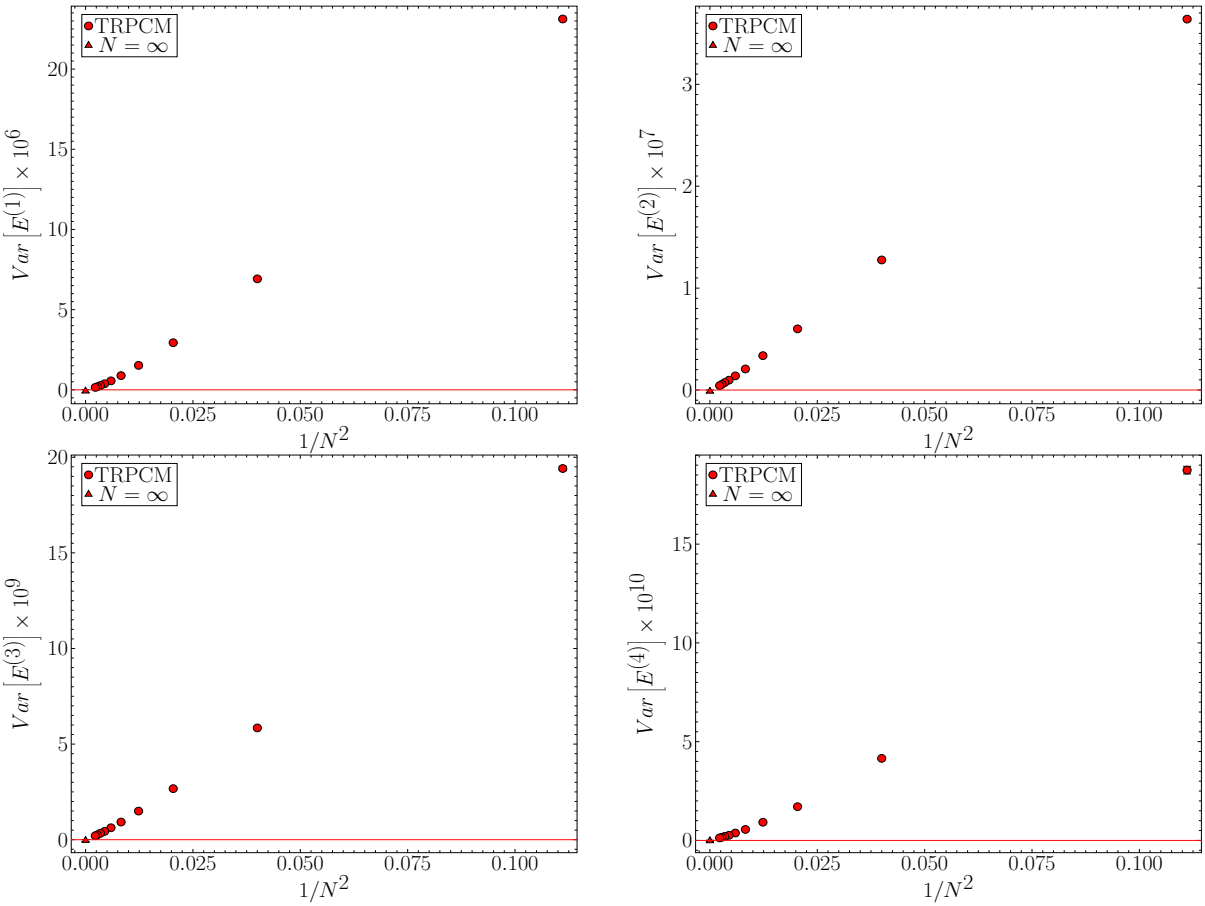

Figure 4: The N dependence of variance of perturbative coefficients of the internal energy up to fourth order.

The statistical error is directly a function of both the variance and the number of statistical (independent) samples, as follows: [78]

$$\left(\delta E^{(k)}\right)^2 = \frac{\mathrm{Var}(E^{(k)})}{N_{\mathrm{sample}}}, \tag{71}$$

where $\delta E^{(k)}$ is the statistical error of $\left\langle E^{(k)} \right\rangle$. The number of independent samples required to achieve a fixed relative statistical error can be estimated as follows:

$$N_{\mathrm{sample}} = \frac{\mathrm{Var}(E^{(k)})}{\left\langle E^{(k)} \right\rangle^2} \left(\frac{\left\langle E^{(k)} \right\rangle}{\delta E^{(k)}} \right)^2. \tag{72}$$

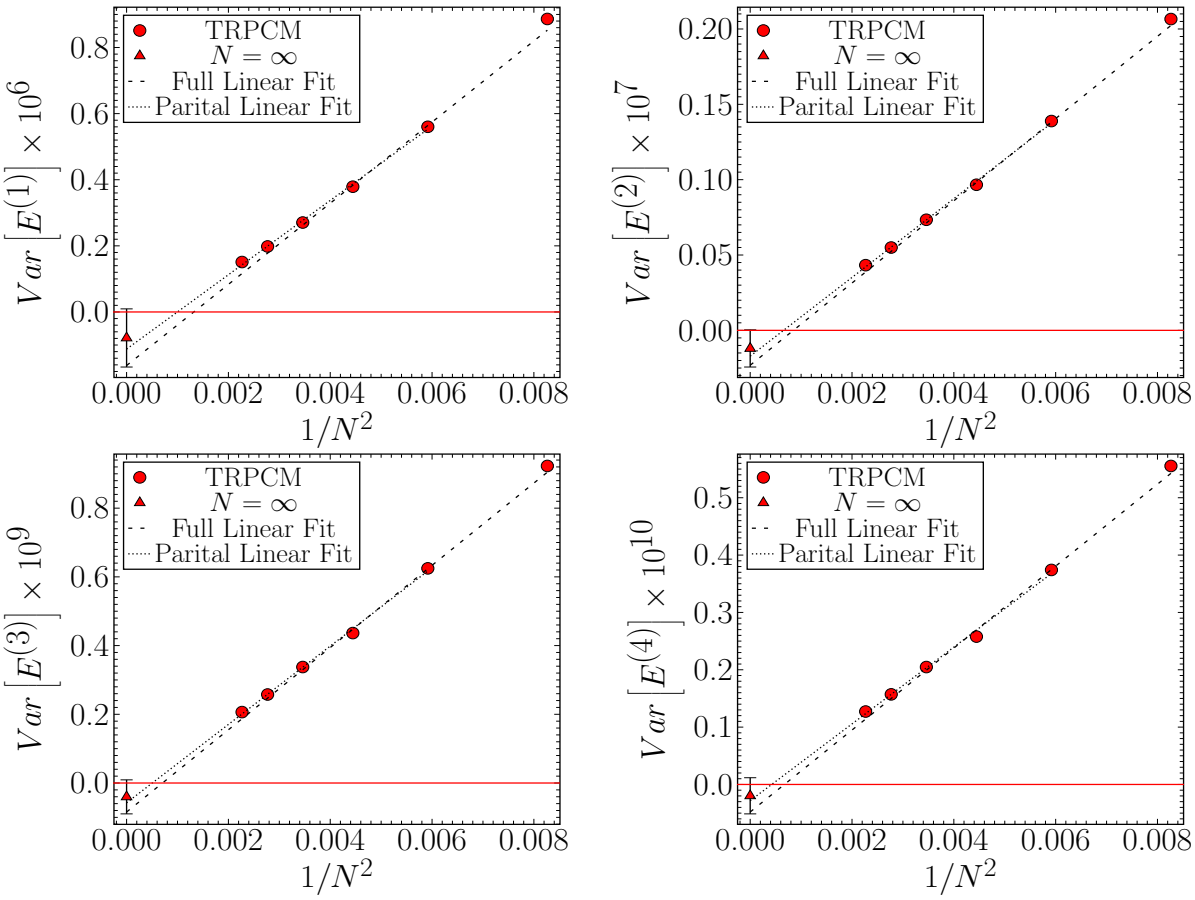

Figure 5: Magnification of Fig. 4 to show the limits as $N \to \infty$.

$\mathrm{Var}(E^{(k)})$ and $\left\langle E^{(k)} \right\rangle$ exhibit the following behavior, as taking the large N limit:

$$\mathrm{Var}(E^{(k)}) \simeq \frac{a^{(k)}}{N^2}, \quad \left\langle E^{(k)} \right\rangle \simeq \left\langle E^{(k)} \right\rangle_\infty + \frac{b^{(k)}}{N^2}. \tag{73}$$

Substituting Eq. (73) into Eq. (72), we have

$$N_{\text{sample}} \simeq \frac{1}{N^2} \frac{a^{(k)}}{\left\langle E^{(k)} \right\rangle_\infty^2} \left(\frac{\left\langle E^{(k)} \right\rangle}{\delta E^{(k)}} \right)^2. \tag{74}$$

If we fix the relative statistical error, the number of independent samples decreases as $1/N^2$, in accordance with the well-known master field property of large N field theory [77]. With slight modifications, the relative statistical error exhibits a linear decrease with increasing N at a fixed

number of independent samples, as:

$$\frac{\delta E^{(k)}}{|\langle E^{(k)}\rangle|} = \frac{\sqrt{\mathrm{Var}(E^{(k)})}}{\sqrt{N_{\mathrm{sample}}}} \simeq \frac{\sqrt{a^{(k)}}}{N\sqrt{N_{\mathrm{sample}}}}. \tag{75}$$

In this subsection, we have examined the finite N correction for each perturbative coefficient of the internal energy. We can estimate the range of N values where the finite N correction is significantly smaller than the statistical error. To estimate the number of statistics required for a single simulation in the large N limit, we will combine two important properties of the large N limit. In addition, it remains unknown that the k-dependence of $a^{(k)}$ and $b^{(k)}$ of Eq. (74). To achieve this, we conducted first fitting on the ratio $-\sqrt{a^{(k)}}/\left\langle E^{(k)}\right\rangle_{\infty}$ as a function of k, using the data for $k > 1$. Our fitting results are displayed in Fig. 6, demonstrating a linear behavior as:

$$\frac{\sqrt{a^{(k)}}}{|\langle E^{(k)}\rangle_{\infty}|} = 0.207k. \tag{76}$$

When analyzing the finite N correction term, $\left|b^{(k)}/(N^2\left\langle E^{(k)}\right\rangle)\right|$, our initial observations based on Eqs. (65) to (68) imply that $|b^{(k)}| \sim |\left\langle E^{(k)}\right\rangle|$, indicating that the finite N correction behaves as $1/N^2$. However, from a Feynman diagrammatic perspective, there is a suggestion that the finite N correction increases as k increases. Consequently, we list two functional forms that describe how $\left|\frac{b^{(k)}}{\langle E^{(k)}\rangle_{\infty}}\right|$ exhibits order dependency as

$$\left|\frac{b^{(k)}}{\langle E^{(k)}\rangle_{\infty}}\right| = 1 \quad \text{or} \quad \left|\frac{b^{(k)}}{\langle E^{(k)}\rangle_{\infty}}\right| = k. \tag{77}$$

Based on these two assumptions, we will now assess the feasibility of a single simulation at a higher order. In this analysis, we choose the order to be $k = 20$, allowing us to observe the renormalon behavior as documented in Ref. [46]. We set the relative error to $\delta E^{(k=20)}/\left|\left\langle E^{(k=20)}\right\rangle\right| = 1\%$, striking a balance between computational time and the confidence of numerical results. As an illustrative example, we will set the value of N to 100.

By utilizing Eqs. (74) and (76), we can calculate the number of independent samples required

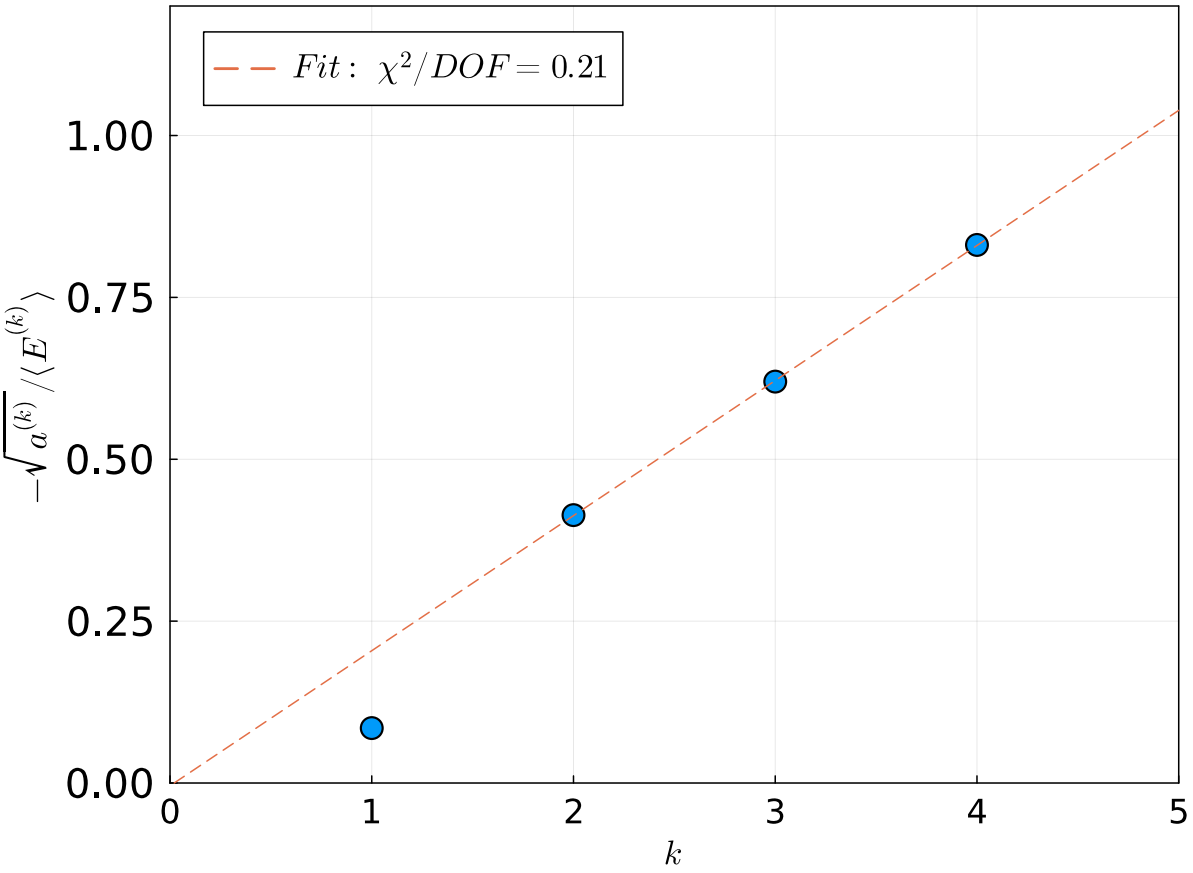

Figure 6: The k dependence of $-\sqrt{a^{(k)}}/\left\langle E^{(k)}\right\rangle_{\infty}$.

to achieve any given statistical error for a given order k, as follows:

$$N_{\text{sample}} \simeq \left(\frac{0.207k}{N}\right)^2 \left(\frac{\left\langle E^{(k)}\right\rangle}{\delta E^{(k)}}\right)^2. \tag{78}$$

By substituting the given parameters, i.e., $k = 20$ and $\delta E^{(k=20)}/\left|\left\langle E^{(k=20)}\right\rangle\right| = 1\%$, into this equation, we obtain $N_{\text{sample}} = 17$. With $N_{\text{sample}} = 17$ for $N = 100$, we demonstrate the possibility that the finite N correction is either comparable to or smaller than the statistical error for each order below $k = 20$.

The upper panel in Fig.7 illustrates the k-dependence of the relative statistical error and the finite N correction with $N = 100$. The blue circles represent the relative statistical error with

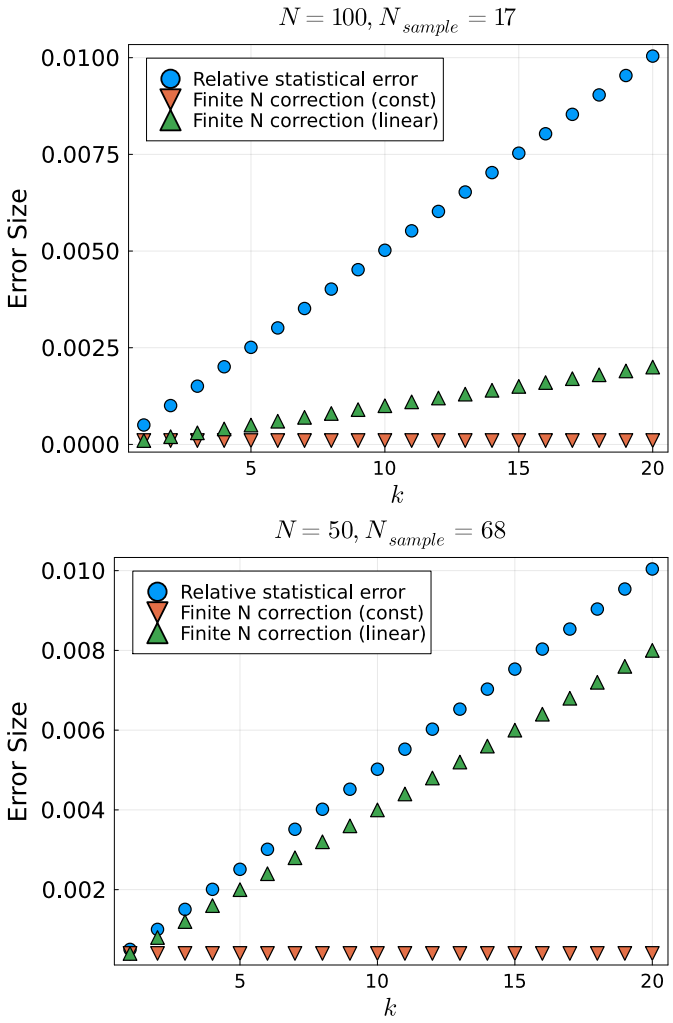

Figure 7: The k dependence of relative statistical error and finite N correction. The number of independent samples is determined by fixing the relative statistical error to be 1% at order $k = 20$.

$N_{\text{sample}} = 17$, set at 1% for $k = 20$. The upward and downward triangles represent the finite N correction under the constant and linear assumptions, respectively, as given in Eq.(77). Both of these finite N corrections are sufficiently smaller than the statistical error, affirming that we can run a single simulation at $N = 100$ with $N_{\text{sample}} = 17$. This allows us to determine the perturbative coefficients up to the 20th order. Using that numerical data, we will report how to extract the signal of renormalons in the next subsection.

Conversely, as N decreases, the finite N correction increases to the point of becoming statistically visible. The panel below in Fig. 7 showcases the k-dependence of the relative statistical

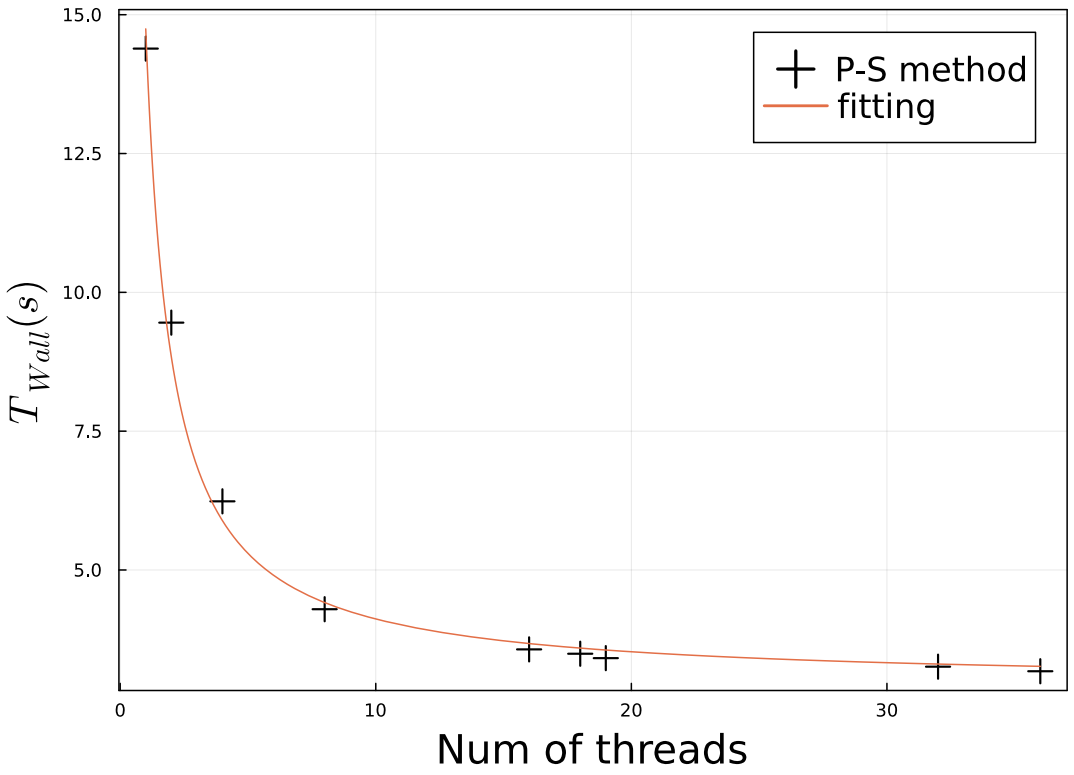

Figure 8: This figure illustrates the thread dependency of computational wall time of the P-S method-based matrix exponential in the NSPT case with $N = 17$.

error and the finite N correction with $N = 50$. The finite N correction, considering a linear dependence, approaches the statistical error. For N values below 50, the finite N correction could become statistically visible under the linear dependence assumption.

To reiterate, by setting the relative statistical error at a high-order coefficient and assuming that the finite N corrections are dependent on k, it is plausible to reach the large N limit with a single NSPT simulation at a sufficiently high N value. We will show the large N results with high-order calculations obtained from the single simulation in Section 4.4.

4.3 Benchmarks of the P-S method

In this subsection, we will demonstrate the improvement in the computation of the matrix exponential for NSPT by presenting benchmark results. This includes analyzing the maximum acceleration benefits derived from using multi-core hardware, examining the time spent running the BATCH-ZGEMM subroutine, and finally comparing the P-S method with Horner's method to validate the theoretical improvements calculated in Section 3.3.

In recent years, a shift in CPU architecture has been observed, transitioning from a focus on increasing clock frequencies to the integration of a greater number of cores, thereby enhancing computational capabilities. The pluralization of computation is now natively supported by both hardware and software.

On the hardware side, pipelines within these instruments enable different operations to be executed simultaneously, and single-instruction, multiple-data (SIMD) capabilities, facilitated by wider registers and instruction set architectures, ensure the simultaneous processing of the same operation on multiple data points. Together with SIMD, current CPU is equipped with multi-core which also enables to execute independent operations or process in parallel.

From a software perspective, an increasing number of application programming interfaces (APIs) have been developed, such as OpenMP [79] and OpenACC [80], to provide developers with simple and flexible interfaces for creating parallel applications across different platforms to make efficiently use of the SIMD and multi-core CPU.

To harness the full computational potential of these multiple cores with instrument level parallelization - SIMD, we initiated a benchmark to evaluate the parallelism of the P-S method. Our investigation begins by applying a modified version of Amdahl's Law, adapted as follows:

$$T_{wall} = t_0 \left[(1 - P) + \frac{P}{\text{num of threads}} \right]. \tag{79}$$

In our notation, T_{wall} represents the total wall time of the matrix exponential computed with a number of parallel threads, t_0 denotes the wall time when using a single thread, and P signifies the proportion of operations that can be parallelized. We conducted a dedicated benchmark of the

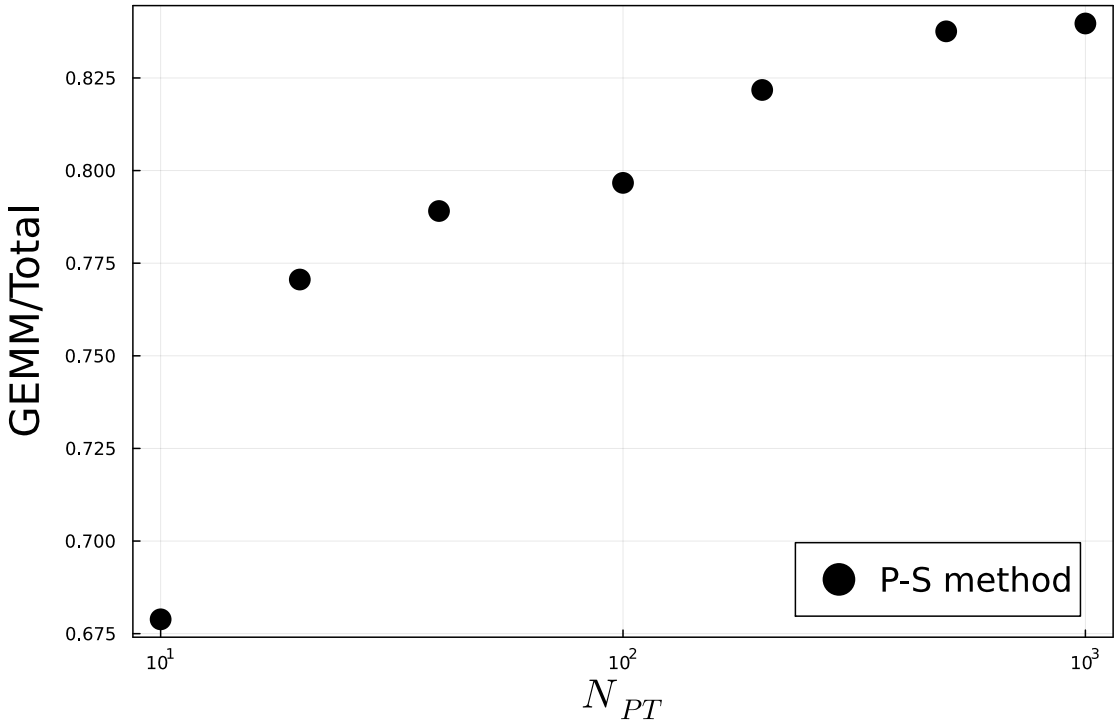

Figure 9: This figure illustrates the proportion of time spent on calling the ZGEMM subroutine in relation to the entire matrix exponential program.

matrix exponential component within the P-S method-based NSPT program, employing various thread counts.

Figure 8 illustrates the total wall time of the matrix exponential function using the P-S method as a function of the number of OpenMP threads with $N = 17$. This wall time corresponds to running the matrix exponential 100 times. By fitting a two-parameter model of Eq. (79) to our observations, we found that approximately $P = 80\%$ of the task can be effectively parallelized. This indicates that if we have infinite hardware's capabilities, a potential speedup by a factor of five will be achievable.

To investigate the source of the high level of parallelization, an additional numerical experiment was conducted. In this experiment, we measured the amount of wall time spent during the

execution of the ZGEMM-BATCH subroutine [72] and subsequently calculated the ratio between this time and the total wall time of the matrix exponential program.

The results are plotted in Fig. 9. Our findings reveal that as the truncated order N_{PT} increases, the time spent on calling ZGEMM-BATCH also increases. This observation leads to the hypothesis that as $N_{\text{PT}} \to \infty$, the time spent in calling ZGEMM-BATCH becomes dominant.

It is noteworthy that ZGEMM-BATCH is a highly parallelized program, suggesting that a significant portion of the observed high parallelization can be attributed to the optimized nature of ZGEMM-BATCH. In specific case that the factorially divergent behavior in the perturbative coefficients can be observed, where the problem size N_{PT} typically ranges from 100 to 1000, approximately 80% of the execution time is devoted to calling ZGEMM-BATCH, showcasing its remarkable efficiency.

Furthermore, as discussed earlier, the P-S method proves to be significantly more efficient than Horner's method. To substantiate this claim, we conducted a numerical experiment on the improvement of adopting the new algorithm. In this specific unit test, we kept the matrix rank fixed at $N = 55$ and configured the number of threads to be 1. The outcomes are presented in Fig. 10.

The upper panel depicts the wall time of both algorithms as we vary the truncation order. As N_{PT} increases, the computation time for both algorithms also increases. However, the P-S method consistently requires less time compared to Horner's method. This implies that for larger values of N_{PT}, utilizing the P-S based method is more efficient, even in the NSPT case.

Moving to the panel below, we showcase the performance enhancement achieved by the new algorithm which is the wall time ratio of the P-S to the Horner's method. After performing a linear regression analysis using all data points, we observe an exponent of approximately -0.42, which is very close to the theoretically expected value of -0.5 estimated in Section 3.3. This indicates significantly faster performance of the P-S method. In addition, we can perform linear regression by excluding the first serval data points. We observe that as more data points are excluded, the slope approaches the theoretical value of -0.5, indicating a significant runtime overhead when N_{PT} is small.

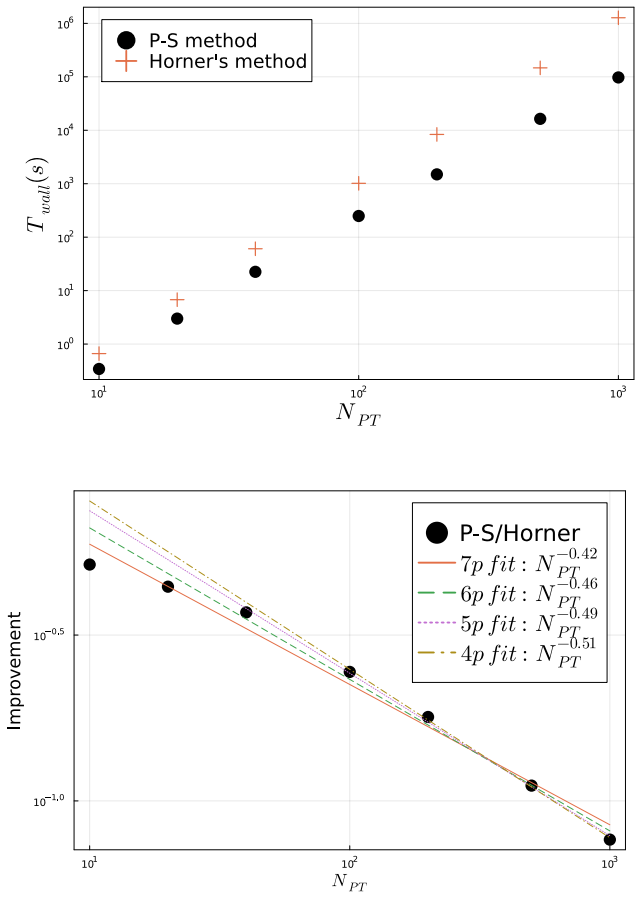

Figure 10: These figures present a comparison between the P-S method and Horner's method-based matrix exponential with $N = 17$. The upper panel displays the wall time of the two algorithms, while the down panel shows the ratio of the wall time of the P-S method to that of Horner's method.

4.4 Large N results at a high-order: single simulation and renormalons

In the preceding subsections, we have demonstrated the large N factorization and the new algorithm to improve the computational complexity in NSPT through the implementation of the newly developed P-S method. Combining these consequences, we can perform high-order calculations at $N \to \infty$ in a reasonable amount of time and examine the existence of renormalons. To do that, we first focus on the perturbative coefficients of the internal energy up to λ^{20}.

Figure 11 shows the perturbative coefficients $\langle E^{(n)} \rangle$ up to λ^{20} for various values of N. It is

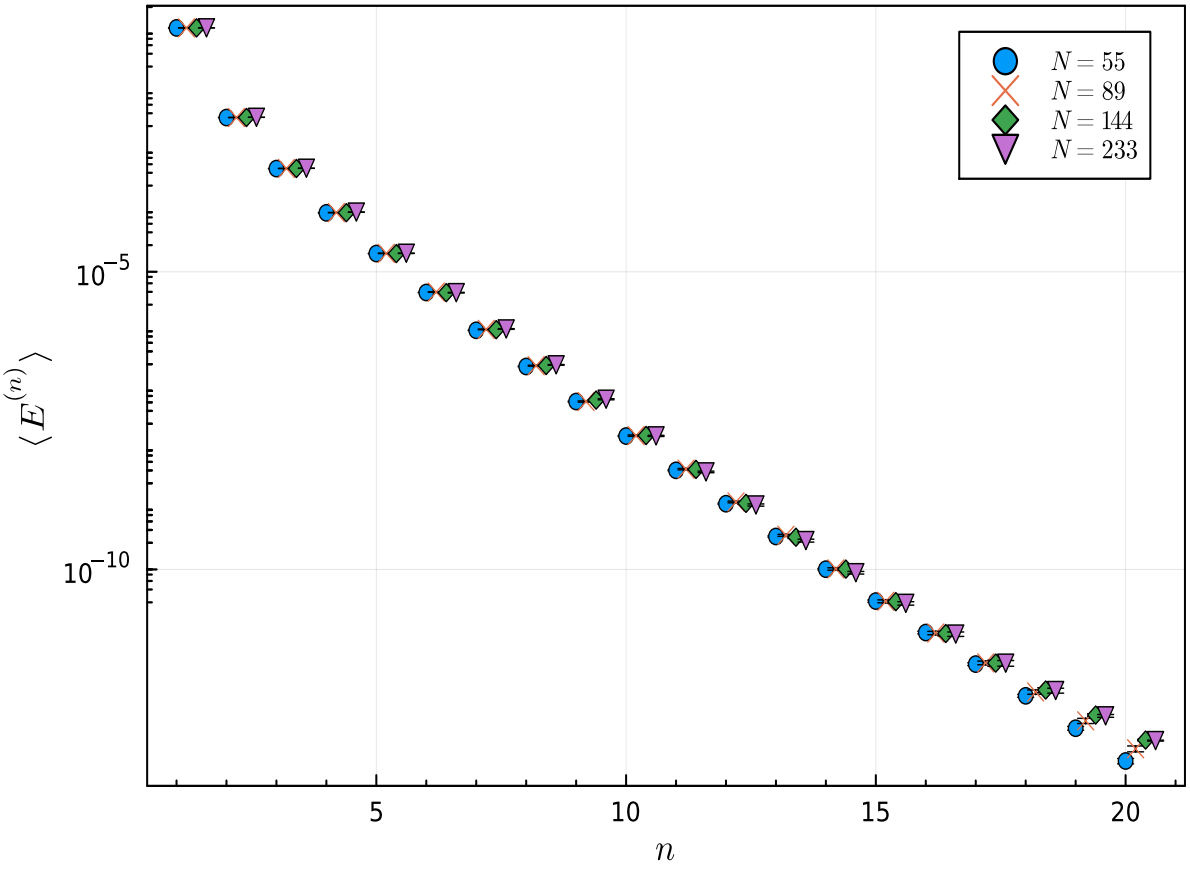

Figure 11: The figure shows the perturbative coefficients up to λ^{20} in log-scale.

evident that even for different values of N, the perturbation coefficients do not exhibit significant dependence on N for low-order terms, up to λ^{15}. This outcome aligns with our previous assumption that $N = 55$ is sufficient to perform a single simulation with our choice of number of samples, and the results are considered to have reached the large N limit.

However, upon examining high-order terms, we observe variations in $E^{(n)}$ with increasing N for the same order. One possible explanation for this behavior is that the volume dependence ($V = L^2 = N^2$) is more pronounced in high-order instances than initially assumed. Utilizing our high-order data, we performed a fitting procedure on Eq.(77) once more, revealing the exponential dependency of order n. Further details are available in Fig.12.

Nonetheless, it is worth noting that as N increases, the value of $E^{(n)}$ converges towards a specific value. This can be observed from the fact that the values of $N = 144$ and $N = 233$ in the

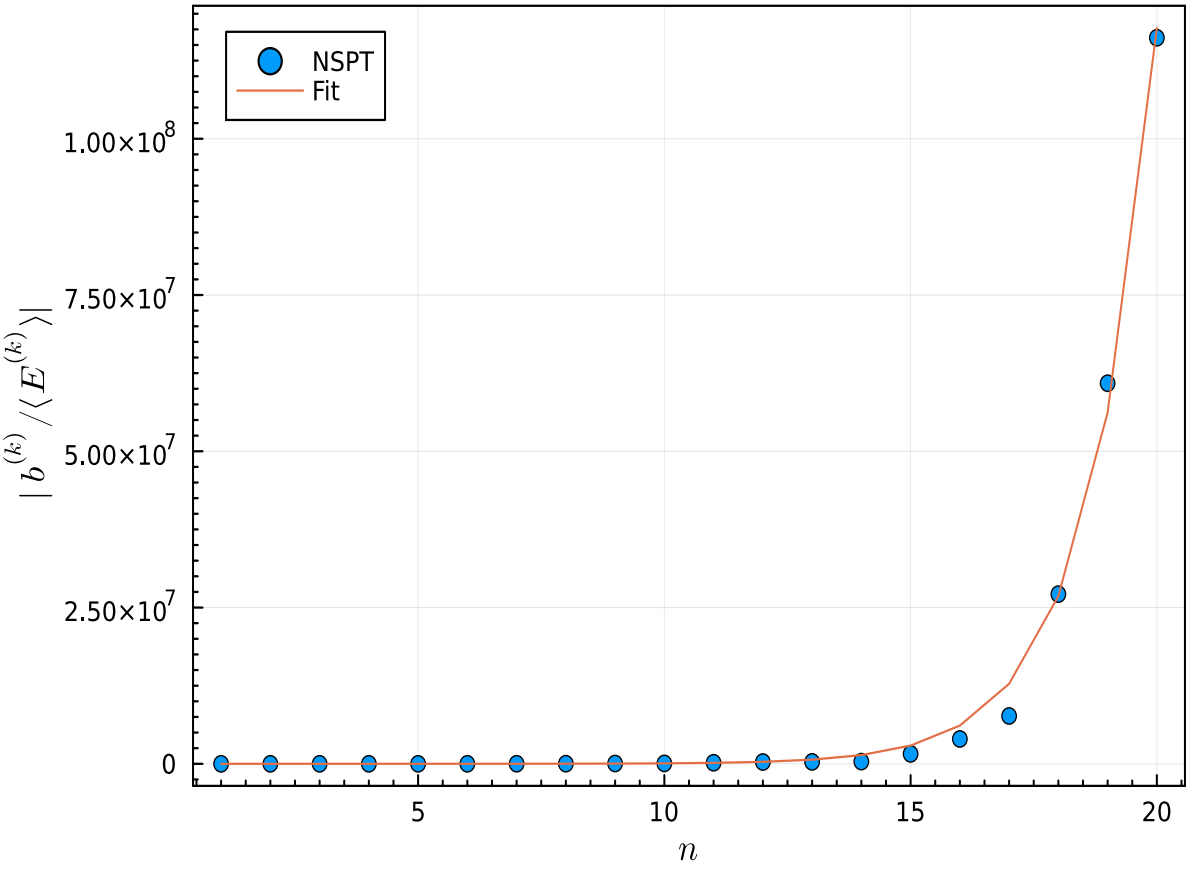

Figure 12: The figure shows a fitting about the exponential order dependency of Eq.(77).

high-order cases are nearly identical. The next observable is the modified ratio, which is defined as

$$r_n = \frac{\langle E^{(n)} \rangle}{\langle n E^{n-1} \rangle}. \tag{80}$$

In the large N limit the modified ratio theoretically converges as

$$\lim_{n\to\infty} r(n) = \frac{1}{16\pi}, \tag{81}$$

from the renormalons argument discussed in Section 2.2. Using the perturbation coefficients obtained from NSPT, we calculate the modified ratio, and the results are shown in Fig. 13.

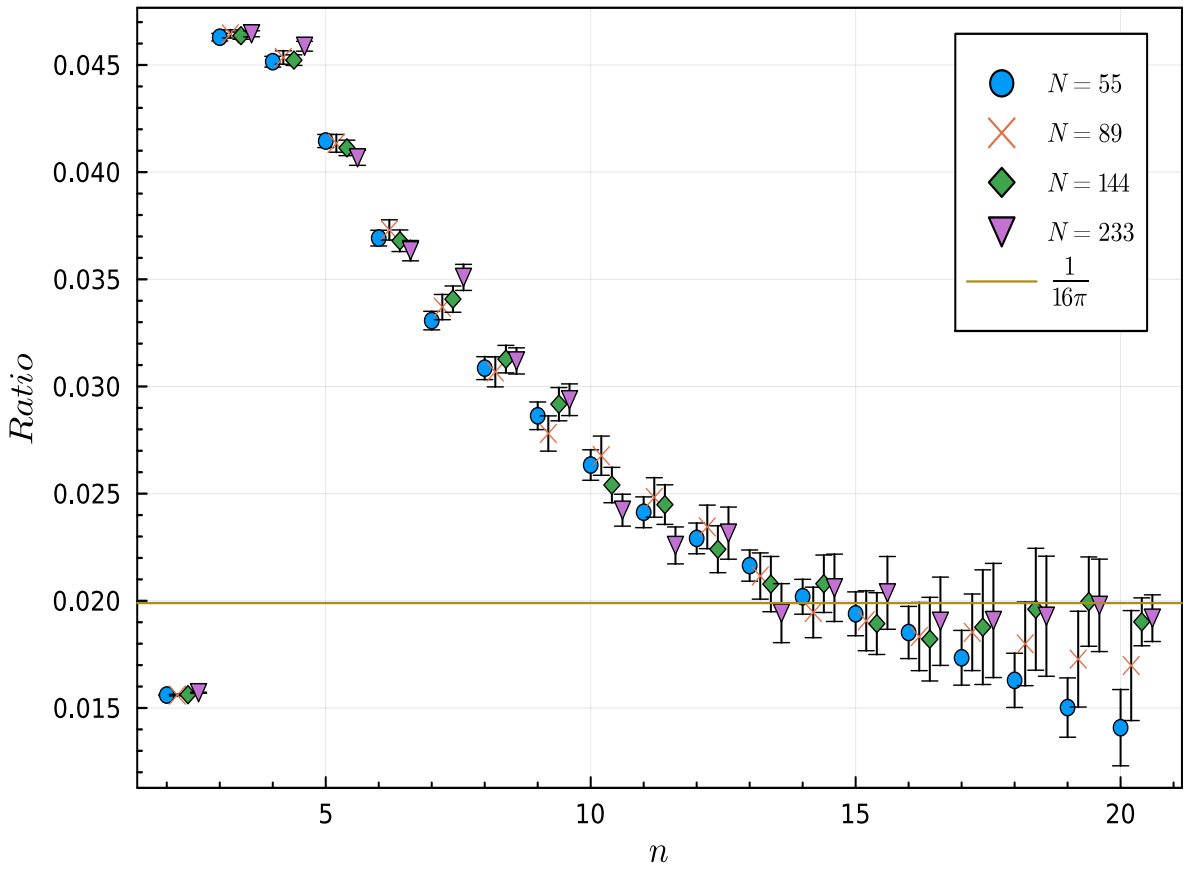

Figure 13: The figure shows the modified ratio defined in Eqs. (80). The horizontal line represents $\frac{1}{16\pi}$.

To verify the N dependence on the modified ratio, we can divide it into two parts for discussion.

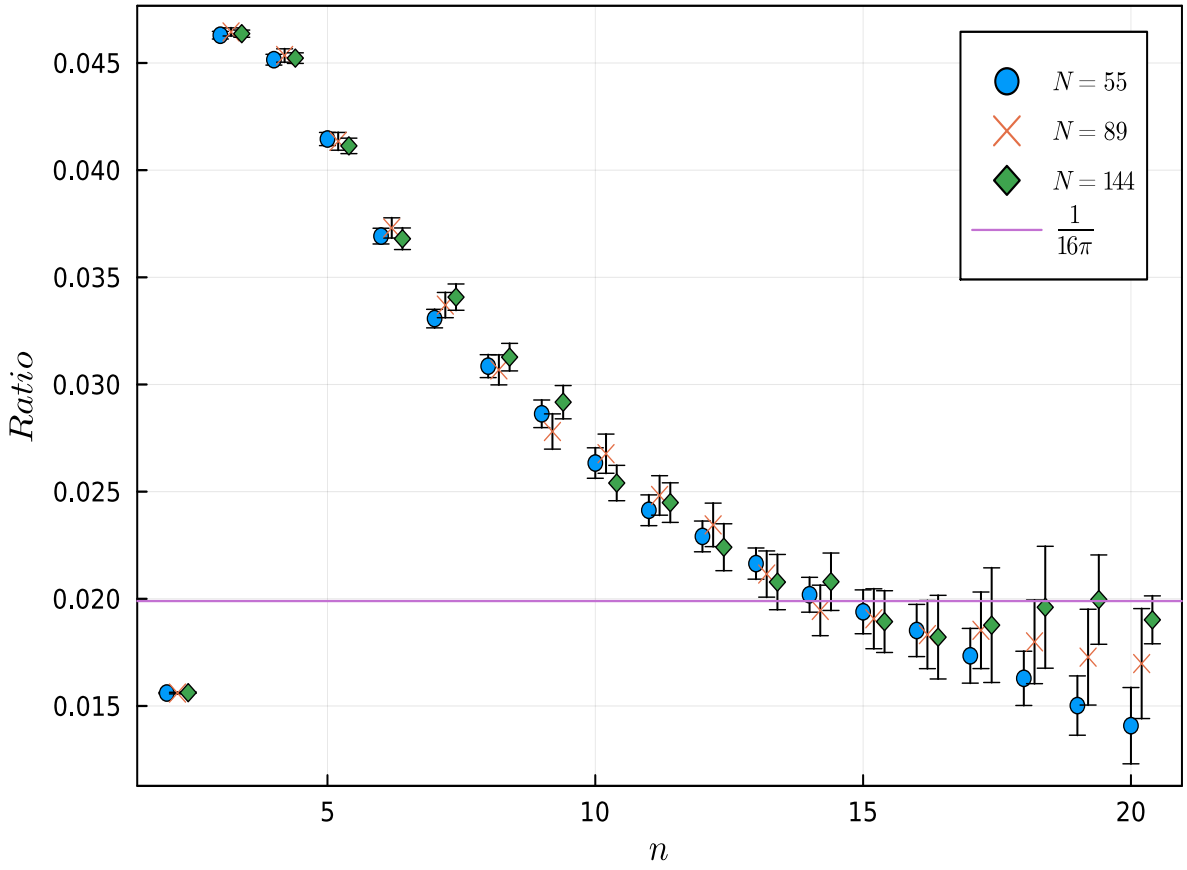

Figure 14: The figure shows the modified ratio defined in Eq. (80) without $N = 233$. The horizontal line represents $\frac{1}{16\pi}$.

Let us start our analysis by turning our attention to Fig. 14 where results with $N = 233$ are removed. In this figure, it is evident that the modified ratio maintains a consistent pattern across various values of N in the lower-order region where $n < 15$. However, as we delve into the high-order domain $n \geq 15$ specifically, the N dependency becomes notably more pronounced.

We observe a discernible trend where the modified ratio for $N = 55$ and $N = 89$ decreases as the order of the expansion increases for $n > 15$. Remarkably, the slope for $N = 89$ appears less steep than that for $N = 55$, indicating a stronger dependency of perturbation coefficients on the system's volume or equally N, particularly in these high-order coefficients.

An intriguing phenomenon appears when $N = 144$ is considered. Here, we witness a conver-

gence of the modified ratio toward a consistent value. Nevertheless, a critical question remains: Is $N = 144$ sufficiently large to accommodate λ^{20} within a "single simulation" ? To address this, we must proceed with our next discussion.

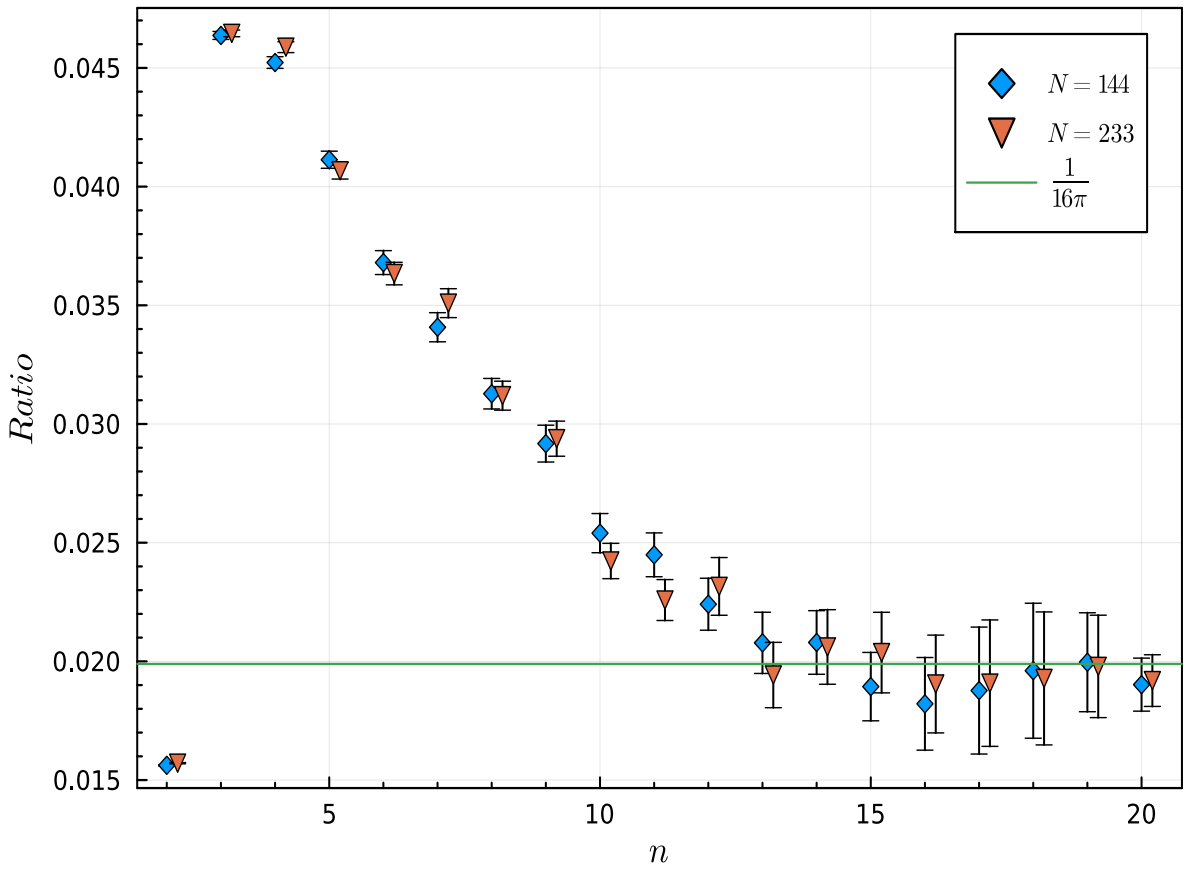

Figure 15: The figure shows the modified ratio defined in Eqs. (80) for $N = 144, 233$. The horizontal line represents $\frac{1}{16\pi}$.

In Fig. 15, we only show the modified ratio for $N = 144$ and $N = 233$ for comparison. Similar to the results observed for the perturbation coefficients in Fig. 11, there is no significant difference in the modified ratio between these two values of N for any order, which confirms that $N = 144$ is indeed large enough to perform a "single simulation" for the internal energy up to λ^{20} order. For the high-order case ($\geq \lambda^{15}$), we observe that the modified ratio oscillates around a constant value of $1/(16\pi)$, indicating convergence to a universal value. This observation is in line

with theoretically expected from renormalons argument in Eq. (81), suggesting the existence of renormalons in the large N limit and providing evidence for the feasibility of a "single simulation" in the TRPCM case.

5 Summary and outlook

Perturbation theory, which involves so many complicated calculations and field variable expanded in terms of a small parameter, provides a straightforward approach to understanding many physical systems from classical system to quantum system. However, the behavior of the perturbation series at high-order can be quite intricate since it may not converge but rather form an asymptotic series. This phenomenon is already evident in relatively simple quantum mechanical systems, such as the an-harmonic oscillator when expanded around trivial vacuum, and even in regular ϕ^4 non-Gaussian integrals , which serve as toy models for path integrals. The same things happen in the realm of quantum field theories. The asymptotic nature of an expansion in powers of g, the coupling constant, suggests an ambiguity, first pointed out by F. Dyson [81], and his observation tentatively leads to the conclusion that all the power-series expansions currently used in quantum electrodynamics are divergent after the renormalization of mass and charge. While the divergence does not restrict the accuracy of practical calculations that can be made with the theory, it does raise important questions of principle concerning the nature of the physical concepts upon which the theory is built. Subsequent studies have delved into the factorially growing perturbative coefficients and their relation to mysterious non-perturbative effects.

Motivated by the aforementioned academic interests and the growing applications of resurgence theory, I conducted an investigation into the non-perturbative nature of TRPCM, employing tools such as NSPT, the large N limit and twisted reduction. Consequently, I successfully discerned the anticipated behavior utilizing the perturbative coefficients of the internal energy. Furthermore, I developed a new algorithm, called the P-S method, for computing the matrix exponential. Benchmark results demonstrate that the P-S method allows us to achieve higher speeds than the commonly used Horner's method, indicating its significance in high-order simulations.

For future studies, there are numerous alternatives to consider. From a physics perspective, the TEK model shares many similarities with TRPCM since they both involve the large N limit, large N factorization enabling us to perform the single simulation, and exhibit asymptotic freedom. The TEK model, identical to the $SU(N)$ pure Yang-Mills theory, has the potential to provide more

comprehensive insights into physics compared to the TRPCM. For example, in the large N limit of the full QCD theory, the fermion becomes decoupled from gluons and exhibits similar physical properties as the TEK model.

However, from a computational perspective, the TEK model is more complicated because it involves four dynamic field variable, whereas the TRPCM only deals with one. Furthermore, the effective volume is different in two models, where $L = N$ in the TRPCM while $L = \sqrt{N}$ in the TEK model. Given that, in TEK model, in order to perform the single simulation, larger N will be required.

Additionally, to extract non-perturbative information from the numerical data of perturbation coefficient in the asymptotically divergent region, one must develop a novel numerical resummation scheme. Traditional methods like Borel resummation are effective for total series but may not be suitable for truncated series and analytic values. We have attempted to achieve this by employing specific special functions. While it worked well for the Gross-Witten-Wadia (GWW) model, it encountered challenges when applied to our high-order numerical data.

The last challenge pertains to the numerical simulation, particularly the computational time. As discussed in Section 4.3, the implementation of a new and more efficient algorithm has led to a decrease in computational time. Another bottleneck in the NSPT program is associated with computing the convolution of two perturbative series defined in Eq.(41). To address this, an alternative has been developed [82], which is based on the first Fourier transformation convolution algorithm. We anticipate that more effective algorithms will be developed in the future.

6 Acknowledgement

I wish to express my deepest gratitude to those who have played a pivotal role in the completion of this doctoral thesis.

Foremost, I extend my sincere appreciation to my supervisor Ken-ichi Ishikawa for his invaluable guidance and scholarly insights. Their expertise and mentorship were indispensable in shaping the theoretical framework of my research. I am indebted to my collaborators Prof. Masanori Okawa and Antonio González-Arroyo. Their intellectual contributions, insightful discussions, and collaborative spirit have enriched my understanding and greatly influenced the development of my work.

I would also like to acknowledge my colleagues in the Theoretical Particle and Hadron Physics Group at Hiroshima University. In particle physics, where the laboratory is the realm of abstract thought, the collective wisdom of those who have delved into the mysteries of the universe is invaluable. I extend my appreciation to the broader scientific community for fostering an environment of collaboration and knowledge sharing

Special thanks go to my family and friends for their unwavering encouragement and understanding throughout this intellectual journey. Their steadfast support has been my anchor during the challenging phases of my research.

I am grateful to everyone who has contributed to the realization of this thesis, marking the culmination of years of dedication and passion for particle physics.

The computation was carried out using the computer resource offered under the category of General Projects by Research Institute for Information Technology, Kyushu University.

A Internal energy in TRPCM

n this appendix, we will describe the analytical part of perturbative calculations in TRPCM and compare some results to lattice PCM to demonstrate the equivalence of the two models, especially in the large N limit. This discussion is based on the private note provided by my collaborator, Antonio González-Arroyo [83] and the textbook of my other collaborators [84].

We start with d (the space-time dimension) $N \times N$ matrices Γ_μ that satisfy the twisted algebraic relation

$$\Gamma_\mu \Gamma_\nu = e^{2\pi i n_{\mu\nu}/N} \Gamma_\nu \Gamma_\mu.$$

In two dimensions, $n_{\mu\nu} = K\epsilon_{\mu\nu}$, where k is an integer coprime with N and $\epsilon_{\mu\nu}$ is a anti-symmetric tensor ($\epsilon_{12} = -\epsilon_{21}$=1). As usual, we will also need its modular inverse integer $\bar{K}$ satisfying $K\bar{K} = 1 \bmod N$. We can introduce the dual basis $\hat{\Gamma}(p)$ that satisfies

$$\Gamma_\mu \hat{\Gamma}(p) \Gamma_\mu^\dagger = e^{ip^\mu} \hat{\Gamma}(p),$$

from matrix product of Γ_μ, where the 2-dimensional integer vectors p can take N^2 values, and the set of matrices with $p \neq 0$ defines a basis for the $SU(N)$ Lie algebra. In 2-dimensions, $p = (2\pi n_1/N, 2\pi n_2/N)$, where n_i are integers modulo N. The components of p are denoted by superscripts $p^\mu = 2\pi n_\mu/N$. We normalize the matrices as follows:

$$\mathrm{Tr}\left(\hat{\Gamma}(p)\hat{\Gamma}^\dagger(p)\right) = \frac{1}{2},$$

This defines the matrices up to multiplication by a phase. Moreover, we can also express

$$\hat{\Gamma}(-p) = e^{i\alpha(p)} \hat{\Gamma}^\dagger(p),$$

where $\alpha(p)$ depends on the chosen phases. For all calculations, one needs to compute traces of products of the $\hat{\Gamma}(p)$. This defines vertex functions as follows:

$$V\left(p_1, p_2, \ldots p_s\right) \equiv \mathrm{Tr}\left(\hat{\Gamma}\left(p_1\right)\hat{\Gamma}\left(p_2\right)\cdots\hat{\Gamma}\left(p_s\right)\right).$$

Typically, in a diagram, these vertex functions need to be computed by joining the momenta in pairs with propagators. Planar diagrams are those in which these lines do not intersect. For our calculation up to order λ^2, we will require a planar vertex

$$V(p,-p,q,-q) = \frac{1}{4N}e^{i\alpha(p)+i\alpha(q)},$$

and a non-planar one

$$V(p,q,-p,-q) = \frac{1}{4N}e^{i\alpha(p)+i\alpha(q)}\cos\left(\frac{N\bar{k}\left(p^1q^2-p^2q^1\right)}{2\pi}\right).$$

A.1 The action in perturbation theory

The partition function of the twisted reduced principal chiral model is given by

$$Z = \int dU \exp\left\{\frac{N}{g^2}\sum_{\mu}\mathcal{P}_{\mu}\right\},$$

where U is an $\mathrm{SU(N)}$ matrix and

$$\mathcal{P}_{\mu} = \frac{1}{N}\mathrm{Tr}\left(U\Gamma_{\mu}U^{\dagger}\Gamma_{\mu}^{\dagger}\right) + \frac{1}{N}\mathrm{Tr}\left(U^{\dagger}\Gamma_{\mu}U\Gamma_{\mu}^{\dagger}\right),$$

which is real. This form is identical to and modified from Eq. (11) for convenience in perturbation calculation. The minimum of the action, the perturbation vacuum,is attained for $U = z\mathbf{I}$, where $\mathbf{I}$ is the unit matrix multiplied by an element of the center $z \in SU(N)$. It is worth noting that for the vacuum solution, the integrand of the partition function becomes $\exp(2dN/g^2)$. In perturbative calculations, all values of z yield equal results, so we will set $z = 1$.

In the following contents, we will compute the action using perturbation theory and it is better to divide the action into 3 parts

$$S = S_0 + S_I + S_M$$

where the S_0 is the free part of the action which contains the kinetic term, the S_I is the interaction part and S_M is from the Haar measure. Then we can expand U around the minimum action solution by writing

$$U = e^{-igA},$$

where A is trace-less hermitian. We then expand the action as a power series in g. The quadratic term in A is independent of g and defines the kinetic term

$$S_0 = \sum_{\mu} \mathrm{Tr}\left(A_{;\mu}^2\right),$$

where we introduced the notation:

$$A_{;\mu} = \Gamma_\mu A \Gamma_\mu^\dagger - A.$$

The remaining portion of the action contains positive powers of g^2 and defines the interacting part S_I. The final step is to expand the matrix A in the basis $\hat{\Gamma}(p)$ as follows:

$$A = \sum_{p}{}' \hat{A}(p)\hat{\Gamma}(p),$$

where the primed summation indicates that the sum excludes $p = 0$. The coefficients $\hat{A}(p)$ are, in principle, complex. The kinetic term can be expressed in terms of them as follows

$$S_0 = \frac{1}{2}\sum_{\mu}\sum_{p}\left|e^{ip^\mu} - 1\right|^2 |\hat{A}(p)|^2 = \frac{1}{2}\sum_{p} e^{i\alpha(p)}\hat{A}(p)\hat{A}(-p)\left(2\sum_{\mu}\left(1 - \cos\left(p^\mu\right)\right)\right),$$

and

$$\sum_{\mu}\left(1 - \cos\left(p^\mu\right)\right) = \sum_{\mu}\left(2\sin\left(p^\mu\right)\right) = \sum_{\mu}\left(\tilde{P}_\mu{}^2\right)$$

This quadratic action defines a Gaussian measure

$$Z_0 = \prod_p{}' \left(\int d\hat{A}(p) \right) e^{-S_0},$$

and expectation values with respect to this measure are labelled by a subscript 0 :

$$\langle O \rangle_0 = \frac{1}{Z_0} \prod_p{}' \left(\int d\hat{A}(p) \right) O e^{-S_0}.$$

Thus, with this measure we define the propagator as

$$\langle \hat{A}(p)\hat{A}(q) \rangle_0 = \delta(p+q)\mathbf{P}(p)e^{-i\alpha(p)}$$

with

$$\mathbf{P}(p) = \frac{1}{2\sum_\mu (1-\cos(p^\mu))} \equiv \frac{1}{D(p)}.$$

Note that in the original partition function, one integrates over dU, the Haar measure of the group, while in the Gaussian theory, one integrates over the coefficients $\hat{A}(p)$. This change of variables gives rise to a Jacobian that we express as follows:

$$dU = g^{N^2-1} \prod_p{}' (d\hat{A}(p)) e^{-S_M},$$

which defines the so-called measure action S_M. This measure is, in fact, the square root of the determinant of the metric tensor g corresponding to the $\mathrm{SU(N)}$ group:

$$ds^2 = \sum_{p,q}{}' g(p,q) d\hat{A}(p) d\hat{A}(q).$$

Thus the measure action is

$$e^{-S_M} = \sqrt{\det(g)} = \exp\left\{ \frac{1}{2} \operatorname{Tr}(\log(g)) \right\},$$

and the metric is given by

$$g(p,q) = 2 \operatorname{Tr} \left(\frac{\partial U}{\partial \hat{A}(p)} \frac{\partial U^\dagger}{\partial \hat{A}(q)} \right),$$

where the unitary matrix is denoted as $U = e^{-igA}$. Consequently, one also needs to expand the measure as a power series in g. The formulas for this expansion can be found in the paper on perturbative expansion on Wilson loops [85]. In leading order, one obtains:

$$S_M = \frac{\lambda}{24} \sum_q{}' \hat{A}(q)\hat{A}(-q)e^{i\alpha(q)} + \mathcal{O}\left(\lambda^2\right).$$

We have expressed the result in terms of the 't Hooft coupling $\lambda = g^2 N$.

A.2 Computing the internal energy

As usual, the internal energy can be obtained by taking the derivative of the partition function with respect to $1/g^2$, yielding the following:

$$E = \frac{1}{2d}\left\langle \sum_\mu \mathcal{P}_\mu \right\rangle = \frac{1}{2dN}\frac{\partial \log Z}{\partial 1/g^2}.$$

Utilizing the results from the previous sections, we can rewrite the partition function as:

$$Z = g^{N^2-1} \prod_p{}' \left(\int d\hat{A}(p) \right) \exp\left\{ 2dN/g^2 - S_0 - S_M - S_I \right\}.$$

where S_0 and S_M are obtained from previous subsections and S_I will be introduced in the next part. Now, perturbation theory involves expressing this formula in terms of the Gaussian partition function:

$$Z = Z_0 g^{N^2-1} e^{2dN/g^2} \left\langle \exp\left\{ -S_M - S_I \right\} \right\rangle_0.$$

From here we conclude

$$E = 1 - \frac{\lambda}{4d}\frac{N^2-1}{N^2} - \frac{\lambda^2}{2dN^3}\frac{\partial \log\left(\left\langle \exp\left\{ -S_M - S_I \right\} \right\rangle_0 \right.}{\partial g^2},$$

where the second term is actually as same as the λ level of internal energy of PCM in Eq. (62).

A.3 Computation to order λ^2

Both S_M and S_I start their expansion up to order g^2, so at this order, we can simply write

$$\langle \mathcal{P} \rangle = 1 - \frac{\lambda}{4d} \frac{N^2 - 1}{N^2} + \frac{\lambda^2}{2dN^2} \frac{\partial \langle (S_M + S_I) \rangle_0}{\partial \lambda},$$

and keep only terms of order g^2 in $(S_M + S_I)$. First, we can compute the contribution of the measure, which was given earlier up to this order

$$S_M = \frac{\lambda}{24} \sum_q{}' \hat{A}(q) \hat{A}(-q) e^{i\alpha(q)}.$$

Thus, the contribution to the internal energy is

$$\frac{\lambda^2}{48dN^2} \sum_q{}' \frac{1}{2 \sum_\mu (1 - \cos(q^\mu))} = \frac{\lambda^2}{48d} X(d, \hat{L}),$$

where we introduced the tadpole integral

$$X(d, \hat{L}) = \frac{1}{N^2} \sum_q{}' \frac{1}{2 \sum_\mu (1 - \cos(q^\mu))}$$

This integral diverges logarithmically as $\hat{L}$ goes to infinity for $d = 2$. The next term arises from S_I up to order λ, and is given by the following expression:

$$\frac{\lambda}{N} \sum_\mu \left(-\frac{4}{4!} \operatorname{Tr}\left(A^4\right) + \frac{2}{3!} \operatorname{Tr}\left(A \Gamma_\mu A^3 \Gamma_\mu^\dagger + \text{hc}\right) - \frac{2}{4} \operatorname{Tr}\left(A^2 \Gamma_\mu A^2 \Gamma_\mu^\dagger\right) \right).$$

Expanding A in the basis $\hat{\Gamma}(p)$,the term in parenthesis becomes

$$\sum_{p_1, p_2, p_3, p_4} A(p_1) A(p_2) A(p_3) A(p_4) V(p_1, p_2, p_3, p_4) \left(-\frac{1}{6} + \frac{2}{3} \cos(p_1^\mu) - \frac{1}{2} \cos(p_1^\mu + p_2^\mu) \right).$$

Then we perform the contractions involved in $\langle A(p_1) A(p_2) A(p_3) A(p_4) \rangle_0$. This decompo-

sition consists of a planar part and a non-planar one. In the planar part, contractions occur among contiguous A:

$$\left\langle A\left(p_1\right)A\left(p_2\right)\right\rangle_0\left\langle A\left(p_3\right)A\left(p_4\right)\right\rangle_0+\left\langle A\left(p_4\right)A\left(p_1\right)\right\rangle_0\left\langle A\left(p_2\right)A\left(p_3\right)\right\rangle_0.$$

Combining this with the trace V one gets

$$\frac{1}{4N}\sum_{p_1}\sum_{p_3}\mathbf{P}\left(p_1\right)\mathbf{P}\left(p_3\right)+\frac{1}{4N}\sum_{p_1}\sum_{p_2}\mathbf{P}\left(p_1\right)\mathbf{P}\left(p_3\right).$$

Then putting together all the terms one gets

$$\frac{\lambda}{4N^2}\sum_{\mu}\sum_{p_1}{}'\sum_{p_2}{}'\left(\frac{-1+4\cos\left(p_1^\mu\right)}{3D\left(p_1\right)D\left(p_2\right)}-\frac{1+\cos\left(p_1^\mu+p_2^\mu\right)}{2D\left(p_1\right)D\left(p_2\right)}\right),$$

and writing the numerator in terms of $D_\mu(p)=2\left(1-\cos\left(p^\mu\right)\right)$ we get

$$-\frac{\lambda}{4N^2}\left(N^2-1\right)\left(\frac{N^2X}{6}+\frac{N^2-1}{8d}\right).$$

Notice that the term involving the logarithmically divergent tadpole, $-\frac{(N^2-1)X}{24N^2}$, partially cancels with the one coming from the measure, resulting in the following at order λ^2:

$$E^{(2)}_{\text{planar}}=\frac{1}{2d}\left(\frac{X}{24N^2}-\frac{1}{32d}\left(1-\frac{1}{N^2}\right)^2\right).$$

We see that this provides the correct leading term, but the correction involves a $\log(N)/N^2$ dependence. Let us now proceed to compute the non-planar part. We have

$$\left\langle A\left(p_1\right)A\left(p_3\right)\right\rangle_0\left\langle A\left(p_2\right)A\left(p_4\right)\right\rangle_0 V\left(p_1,p_2,p_3,p_4\right)Q\left(p_1,p_2\right),$$

where

$$Q\left(p_1,p_2\right)=\sum_{\mu}\left(-\frac{1}{6}+\frac{2}{3}\cos\left(p_1^\mu\right)-\frac{1}{2}\cos\left(p_1^\mu+p_2^\mu\right)\right).$$

Substituting the expression of the propagators, we obtain

$$\delta\left(p_1+p_3\right)\delta\left(p_2+p_4\right)\mathbf{P}\left(p_1\right)\mathbf{P}\left(p_2\right)V\left(p_1,p_2,-p_1,-p_2\right)e^{-i\alpha(p_1)-i\alpha(p_2}Q\left(p_1,p_2\right).$$

Finally collecting all the factors together we get the non-planar contribution (for $\mathrm{d}=2$)

$$E^{(2)}_{\text{non-planar}}=\frac{1}{16N^4}\sum_{p}^{'}\sum_{q}^{'}\mathbf{P}(p)\mathbf{P}(q)Q(p,q)\cos\left(\frac{N\bar{k}\left(p^1q^2-p^2q^1\right)}{2\pi}\right).$$

The non-planar part tends to zero as $N\longrightarrow\infty$, as explained in the proof of the volume independence of the twisted reduced models. Furthermore, in the non-planar part, there appears to be a term that cancels the contribution proportional to X from the planar part. This implies that there would be no subleading $\log(N)/N^2$ term, as indicated by the calculation. Thus, the leading correction goes like $1/N^2$, as shown by the numerical results. In summary, we have computed the coefficient $E^{(2)}$ in perturbation theory, given by the sum

$$E^{(2)}=E^{(2)}_{\text{planar}}+E^{(2)}_{\text{non-planar}},$$

which can be easily computed numerically.

B An example of similarities between n-dimensional PCM and $2n$-dimensional gauge theory

In this study, our primary aim is to investigate the perturbative behavior of gauge theories describing the interaction among quarks and gluons in the real world. However, due to the many similarities between gauge theories and PCM, we can extract valuable information from this toy model. In this appendix, we aim to introduce, as the title suggests, the similarities between n-dimensional PCM and $2n$ gauge theory. More detailed information can be found in Ref. [27].

PCM is a unitary matrix model defined on the lattice. Similarly, gauge theory is also a matrix model defined on the lattice. Understanding the connection between these two models will provide additional insights into one model through the lens of the other. In Table 7, we list the relations between$n$-d PCM and $2n$-d gauge theories.

n-d PCM	$2n$ gauge theories
site	link
link	plaquette
mass gap	string tension
two-point function	Wilson loop

Table 7: Similarities between PCM and gauge theories.

To illustrate that, here, we consider a 1-d lattice PCM whose action can be defined as

$$S_{\text{PCM}} = -2N\beta \sum_{x,\mu} \text{Re}\,\text{Tr}\left[U_x U_{x+\mu}^{\dagger}\right], \quad \beta = \frac{1}{Ng^2}. \tag{82}$$

In addition, the 2-d gauge theory is built upon the dynamical variable $U_{x,\mu}$, defined as the link variable and the Wilson lattice action is $S_{\text{Gauge}} = -\beta \sum_x \sum_{\mu,v} = \text{Tr}(U_\mu U_v U_\mu^{\dagger} U_v^{\dagger})$. However, in the 2-d case, various techniques can be employed to simplify the model for analysis, such as fixing

the gauge as

$$U_{x,0} = I, \tag{83}$$

where I denotes the identity matrix, corresponding to the lattice version of the temporal gauge $A_0 = 0$ and $U_{x,0} = e^{igA_0}$. Upon substituting this expression into the definition of the 2-D plaquette, one can obtain

$$\mathrm{Tr}\left(U_{x,0}U_{x+0,1}U^{\dagger}_{x+1,0}U^{\dagger}_{x,1}\right) \to \mathrm{Tr}\, U_{x+0,1}U^{\dagger}_{x,1}, \tag{84}$$

and therefore the action of 2-d gauge theory becomes

$$S = -\beta N \sum_i \mathrm{Tr}\left(U_i U^{\dagger}_{i+1} + U^{\dagger}_i U_{i+1}\right), \tag{85}$$

which is identical to Eq. (82) after re-scaling the coupling constant, even though the definition of the dynamical variable U differs between the two cases.

References

[1] Michael E. Peskin and Daniel V. Schroeder. *An Introduction to quantum field theory*. Addison-Wesley, Reading, USA, 1995.

[2] Gerard 't Hooft. A Planar Diagram Theory for Strong Interactions. *Nucl. Phys. B*, 72:461, 1974.

[3] Tohru Eguchi and Hikaru Kawai. Reduction of dynamical degrees of freedom in the large-n gauge theory. *Phys. Rev. Lett.*, 48:1063–1066, Apr 1982.

[4] Masanori Okawa. Monte Carlo Study of the Eguchi-kawai Model. *Phys. Rev. Lett.*, 49:353, 1982.

[5] Antonio González-Arroyo and M. Okawa. The Twisted Eguchi-Kawai Model: A Reduced Model for Large N Lattice Gauge Theory. *Phys. Rev. D*, 27:2397, 1983.

[6] Antonio González-Arroyo and M. Okawa. A Twisted Model for Large N Lattice Gauge Theory. *Phys. Lett. B*, 120:174–178, 1983.

[7] Kenneth G. Wilson. Confinement of Quarks. *Phys. Rev. D*, 10:2445–2459, 1974.

[8] Michael Creutz. *Quarks, Gluons and Lattices*. Oxford University Press, 1983.

[9] Michael Creutz, Laurence Jacobs, and Claudio Rebbi. Monte Carlo Study of Abelian Lattice Gauge Theories. *Phys. Rev. D*, 20:1915, 1979.

[10] M. Creutz. Monte Carlo Study of Quantized SU(2) Gauge Theory. *Phys. Rev. D*, 21:2308–2315, 1980.

[11] Michael Creutz. Confinement and Lattice Gauge Theory. *Phys. Scripta*, 23:973, 1981.

[12] Heinz J. Rothe. *Lattice Gauge Theories : An Introduction (Fourth Edition)*, volume 43. World Scientific Publishing Company, 2012.

[13] A. Ukawa and M. Fukugita. LANGEVIN SIMULATION INCLUDING DYNAMICAL QUARK LOOPS. *Phys. Rev. Lett.*, 55:1854, 1985.

[14] David J. E. Callaway and Aneesur Rahman. Microcanonical ensemble formulation of lattice gauge theory. *Phys. Rev. Lett.*, 49:613–616, Aug 1982.

[15] S. Duane, A. D. Kennedy, B. J. Pendleton, and D. Roweth. Hybrid Monte Carlo. *Phys. Lett. B*, 195:216–222, 1987.

[16] J. Beringer et al. Review of Particle Physics (RPP). *Phys. Rev. D*, 86:010001, 2012.

[17] S. Durr et al. Ab-Initio Determination of Light Hadron Masses. *Science*, 322:1224–1227, 2008.

[18] Carl M. Bender and Tai Tsun WU. Large order behavior of Perturbation theory. *Phys. Rev. Lett.*, 27:461, 1971.

[19] V. S. Popov, V. L. Eletsky, and A. V. Turbiner. Borel Summation of Perturbation Series in Quantum Mechanics and Field Theory. *Phys. Lett. B*, 72:99–102, 1977.

[20] G. Parisi and Yong-shi Wu. Perturbation Theory Without Gauge Fixing. *Sci. Sin.*, 24:483, 1981.

[21] E. Floratos and J. Iliopoulos. Equivalence of stochastic and canonical quantization in perturbation theory. *Nuclear Physics B*, 214(3):392–404, 1983.

[22] H. Huffel and P. V. Landshoff. Stochastic Diagrams and Feynman Diagrams. *Nucl. Phys. B*, 260:545, 1985.

[23] F. Di Renzo, G. Marchesini, P. Marenzoni, and E. Onofri. Lattice perturbation theory on the computer. *Nucl. Phys. B Proc. Suppl.*, 34:795–798, 1994.

[24] Stefano Profumo. Non-commutative principal chiral models. *Journal of High Energy Physics*, 2002(10):035–035, oct 2002.

[25] Luigi Del Debbio, Haralambos Panagopoulos, Paolo Rossi, and Ettore Vicari. Spectrum of confining strings in SU(n) gauge theories. *Journal of High Energy Physics*, 2002(01):009–009, jan 2002.

[26] J. Shigemitsu, J. B. Kogut, and D. K. Sinclair. Comparing O(N) and SU(N) X SU(N) Spin Systems in (1+1)-dimensions to SU(N) Gauge Theories in (3+1)-dimensions. *Phys. Lett. B*, 100:316–320, 1981.

[27] Paolo Rossi, Massimo Campostrini, and Ettore Vicari. The Large N expansion of unitary matrix models. *Phys. Rept.*, 302:143–209, 1998.

[28] Frederic Green and Stuart Samuel. Chiral Models: Their Implication for Gauge Theories and Large N. *Nucl. Phys. B*, 190:113–150, 1981.

[29] E. Abdalla, M. C. B. Abdalla, and A. Lima-Santos. On the exact S-matrix of the principal chiral model. *Phys. Lett. B*, 140:71–75, 1984. [Erratum: Phys.Lett.B 146, 457–457 (1984)].

[30] P. Wiegmann. EXACT FACTORIZED S MATRIX OF THE CHIRAL FIELD IN TWO-DIMENSIONS. *Phys. Lett. B*, 142:173–176, 1984.

[31] Frederic Green and Stuart Samuel. The Large N Phase Transition in the U(N) Chiral Models. *Phys. Lett. B*, 103:110–112, 1981.

[32] Massimo Campostrini, Paolo Rossi, and Ettore Vicari. Strong coupling expansion of chiral models. *Phys. Rev. D*, 52:358–385, 1995.

[33] Massimo Campostrini, Paolo Rossi, and Ettore Vicari. Large N phase transition in lattice 2-d principal chiral models. *Phys. Rev. D*, 52:395–401, 1995.

[34] J. Balog, S. Naik, F. Niedermayer, and P. Weisz. Exact mass gap of the chiral SU(n) x SU(n) model. *Phys. Rev. Lett.*, 69:873–876, 1992.

[35] P. Rossi and E. Vicari. Two-dimensional SU(N) x SU(N) chiral models on the lattice. *Nucl. Phys. B Proc. Suppl.*, 34:689–691, 1994.

[36] Antonio González-Arroyo and M. Okawa. TWISTED REDUCED CHIRAL MODEL. *Nucl. Phys. B*, 247:104–124, 1984.

[37] Antonio González-Arroyo and Masanori Okawa. The two-dimensional twisted reduced principal chiral model revisited. *JHEP*, 06:158, 2018.

[38] E. Gozzi, C. Pagani, and M. Reuter. The Response Field and the Saddle Points of Quantum Mechanical Path Integrals. *Annals Phys.*, 429:168457, 2021.

[39] Cihan Pazarbaşı and Dieter Van Den Bleeken. Renormalons in quantum mechanics. *JHEP*, 08:096, 2019.

[40] M. Beneke. Renormalons. *Phys. Rept.*, 317:1–142, 1999.

[41] Gerald V. Dunne and Mithat Unsal. Uniform WKB, Multi-instantons, and Resurgent Trans-Series. *Phys. Rev. D*, 89(10):105009, 2014.

[42] Daniele Dorigoni. An Introduction to Resurgence, Trans-Series and Alien Calculus. *Annals Phys.*, 409:167914, 2019.

[43] Gerald V. Dunne and Mithat Ünsal. Continuity and Resurgence: towards a continuum definition of the $\mathbb{CP}$(N-1) model. *Phys. Rev. D*, 87:025015, 2013.

[44] Tatsuhiro Misumi, Muneto Nitta, and Norisuke Sakai. Neutral bions in the $\mathbb{C}P^{N-1}$ model for resurgence. *J. Phys. Conf. Ser.*, 597(1):012060, 2015.

[45] Sergei Gukov, Marcos Marino, and Pavel Putrov. Resurgence in complex Chern-Simons theory. 5 2016.

[46] Falk Bruckmann and Matthias Puhr. Universal Renormalons in Principal Chiral Models. *Phys. Rev. D*, 101(3):034513, 2020.

[47] Matthias Puhr and Falk Bruckmann. A Lattice Study of Renormalons in Asymptotically Free Sigma Models. *PoS*, LATTICE2018:237, 2018.

[48] Jan Fischer. On the role of power expansions in quantum field theory. *Int. J. Mod. Phys. A*, 12:3625–3663, 1997.

[49] Antonio González-Arroyo, Issaku Kanamori, Ken-Ichi Ishikawa, Kanata Miyahana, Masanori Okawa, and Ryoichiro Ueno. Numerical stochastic perturbation theory applied to the twisted Eguchi-Kawai model. *JHEP*, 06:127, 2019.

[50] Antonio González-Arroyo and Masanori Okawa. Large N reduction with the Twisted Eguchi-Kawai model. *JHEP*, 07:043, 2010.

[51] Stefano Profumo and Ettore Vicari. Twisted Eguchi-Kawai reduced chiral models. *JHEP*, 05:014, 2002.

[52] F. Di Renzo, E. Onofri, G. Marchesini, and P. Marenzoni. Four loop result in SU(3) lattice gauge theory by a stochastic method: Lattice correction to the condensate. *Nucl. Phys. B*, 426:675–685, 1994.

[53] Michele Brambilla, Mattia Dalla Brida, Francesco Di Renzo, Dirk Hesse, and Stefan Sint. Numerical Stochastic Perturbation Theory in the Schrödinger Functional. *PoS*, Lattice2013:325, 2014.

[54] Mattia Dalla Brida and Dirk Hesse. Numerical Stochastic Perturbation Theory and the Gradient Flow. *PoS*, Lattice2013:326, 2014.

[55] Clemens Bauer, Gunnar S. Bali, and Antonio Pineda. Compelling Evidence of Renormalons in QCD from High Order Perturbative Expansions. *Phys. Rev. Lett.*, 108:242002, 2012.

[56] Gunnar S. Bali, Clemens Bauer, Antonio Pineda, and Christian Torrero. Perturbative expansion of the energy of static sources at large orders in four-dimensional SU(3) gauge theory. *Phys. Rev. D*, 87:094517, 2013.

[57] Luigi Del Debbio, Francesco Di Renzo, and Gianluca Filaci. Large-order NSPT for lattice gauge theories with fermions: the plaquette in massless QCD. *Eur. Phys. J. C*, 78(11):974, 2018.

[58] Gunnar S. Bali, Clemens Bauer, and Antonio Pineda. Perturbative expansion of the plaquette to $\mathcal{O}(\alpha^{35})$ in four-dimensional SU(3) gauge theory. *Phys. Rev. D*, 89:054505, 2014.

[59] Ryuichiro Kitano, Hiromasa Takaura, and Shoji Hashimoto. Stochastic computation of $g`2$ in QED. *JHEP*, 05:199, 2021.

[60] Mattia Dalla Brida, Marco Garofalo, and A. D. Kennedy. Investigation of New Methods for Numerical Stochastic Perturbation Theory in φ^4 Theory. *Phys. Rev. D*, 96(5):054502, 2017.

[61] Mattia Dalla Brida and Martin Lüscher. SMD-based numerical stochastic perturbation theory. *Eur. Phys. J. C*, 77(5):308, 2017.

[62] Masanori Okawa Ken-Ichi Ishikawa, Yingbo Ji. Fast computing matrix function in numerical stochastic perturbation theory. *Submitting to Springer Proceedings in Physics.*

[63] Paul B. Mackenzie. An Improved Hybrid Monte Carlo Method. *Phys. Lett. B*, 226:369–371, 1989.

[64] A. D. Kennedy and Brian Pendleton. Cost of the generalized hybrid Monte Carlo algorithm for free field theory. *Nucl. Phys. B*, 607:456–510, 2001.

[65] Mattia Dalla Brida, Marco Garofalo, and A. D. Kennedy. Investigation of New Methods for Numerical Stochastic Perturbation Theory in φ^4 Theory. *Phys. Rev. D*, 96(5):054502, 2017.

[66] Michael S. Paterson and Larry J. Stockmeyer. On the number of nonscalar multiplications necessary to evaluate polynomials. *SIAM Journal on Computing*, 2(1):60–66, 1973.

[67] Massimiliano Fasi. Optimality of the paterson–stockmeyer method for evaluating matrix polynomials and rational matrix functions. *Linear Algebra and its Applications*, 574:182–200, 2019.

[68] Jorge Sastre and Javier Ibáñez. Efficient evaluation of matrix polynomials beyond the paterson–stockmeyer method. *Mathematics*, 9(14), 2021.

[69] Antonio González-Arroyo, Ken-Ichi Ishikawa, Yingbo Ji, and Masanori Okawa. Perturbative study of large N principal chiral model with twisted reduction. *Int. J. Mod. Phys. A*, 37(36):2250210, 2022.

[70] Yingbo Ji Masanori Okawa Antonio González-Arroyo, Ken-Ichi Ishikawa. Exacting the renormalons from the perturbation series in twisted reduced principal chiral model. *78th annual meeting(2023), The physical society of Japan*.

[71] Homepage of Ito supercomputer. https://www.cc.kyushu-u.ac.jp/scp/.

[72] Introducing Batch GEMM Operations. https://www.intel.com/content/www/us/en/developer/articles/technic batch-gemm-operations.html.

[73] Paolo Rossi and Ettore Vicari. Two-dimensional SU(N) x SU(N) chiral models on the lattice. 2. The Green's function. *Phys. Rev. D*, 49:6072, 1994. [Erratum: Phys.Rev.D 50, 4718 (1994), Erratum: Phys.Rev.D 55, 1698 (1997)].

[74] P. Rossi and E. Vicari. Two-dimensional SU(N) x SU(N) chiral models on the lattice. *Nucl. Phys. B Proc. Suppl.*, 34:689–691, 1994.

[75] Matthias Puhr and Falk Bruckmann. NSPT-scripts. *NSPT-scripts*, 2019.

[76] Y. Brihaye and P. Rossi. The weak-coupling phase of lattice spin and gauge models. 235(2):226–258, June 1984.

[77] Edward Witten. THE 1 / N EXPANSION IN ATOMIC AND PARTICLE PHYSICS. *NATO Sci. Ser. B*, 59:403–419, 1980.

[78] Frederik Dekking, Cor Kraaikamp, Hendrik Lopuhaä, and Ludolf Meester. *A Modern Introduction to Probability and Statistics, Understanding Why and How*. 01 2005.

[79] OpenMP API 5.2 Specification. https://www.openmp.org/wp-content/uploads/OpenMP-API-Specification-5-2.pdf.

[80] The OpenACC Application Programming Interface Version 3.1. https://www.openacc.org/sites/default/files/inline-images/Specification/OpenACC-3.1-final.pdf.

[81] F. J. Dyson. Divergence of perturbation theory in quantum electrodynamics. *Phys. Rev.*, 85:631–632, Feb 1952.

[82] Antonio González-Arroyo, Issaku Kanamori, Ken-Ichi Ishikawa, Kanata Miyahana, Masanori Okawa, and Ryoichiro Ueno. Towards higher order numerical stochastic perturbation computation applied to the twisted Eguchi-Kawai model. *PoS*, LATTICE2019:030, 2019.

[83] Antonio González-Arroyo. Private note.

[84] Masanori Okawa Ken-Ichi Ishikawa. 格子場の理論入門. サイエンス社,*SGC*ライブラリ *140*.

[85] Margarita García Pérez, Antonio González-Arroyo, and Masanori Okawa. Perturbative contributions to Wilson loops in twisted lattice boxes and reduced models. *JHEP*, 10:150, 2017.